NASA CR-142855
ERIM 193300-32-F

Final Report

SURFACE COMPOSITIONAL MAPPING BY SPECTRAL RATIOING OF ERTS-1 MSS DATA IN THE WIND RIVER BASIN AND RANGE, WYOMING

R.K. VINCENT, B.C. SALMON,
W.W. PILLARS and J.E. HARRIS
Infrared and Optics Division

JUNE 1975

(E75-10312) SURFACE COMPOSITIONAL MAPPING BY SPECTRAL RATIOING OF ERTS-1 MSS DATA IN THE WIND RIVER BASIN AND RANGE, WYOMING Final Report, Sep. 1972 - Sep. 1974 (Environmental Research Inst. of Michigan) G3/43 N75-25259 Unclas 00312

Prepared for

NATIONAL AERONAUTICS AND SPACE ADMINISTRATION

Goddard Space Flight Center
Greenbelt, Maryland 20771
Contract No. NAS5-21783, Task X
E. F. Szajna, Technical Monitor Code 430

ENVIRONMENTAL
RESEARCH INSTITUTE OF MICHIGAN
FORMERLY WILLOW RUN LABORATORIES THE UNIVERSITY OF MICHIGAN
BOX 618 • ANN ARBOR • MICHIGAN 48107

NOTICES

Sponsorship. The work reported herein was conducted by the Environmental Research Institute of Michigan for the National Aeronautics and Space Administration, Goddard Space Flight Center, Greenbelt, Maryland, 20771, under Contract NAS5-21783 Task X. Mr. E.F. Szajna Code.430 was Technical Monitor. Contracts and grants to the Institute for the support of sponsored research are administered through the Office of Contracts Administration.

Availability Notice. Requests for copies of this report should be referred to:

National Aeronautics and Space Administration
Scientific and Technical Information Facility
P.O. Box 33
College Park, Maryland 20740

TECHNICAL REPORT STANDARD TITLE PAGE

1. Report No. NASA CR-ERIM 193300-32-F	2. Government Accession No.	3. Recipient's Catalog No
4. Title and Subtitle SURFACE COMPOSITIONAL MAPPING BY SPECTRAL RATIOING OF ERTS-1 MSS DATA IN THE WIND RIVER BASIN AND RANGE, WYOMING		5. Report Date June 1975
		6. Performing Organization Code
7. Author(s) R.K. Vincent, B.C. Salmon, W.W. Pillars and J.E. Harris		8. Performing Organization Report No. 193300-32-F
9. Performing Organization Name and Address Environmental Research Institute of Michigan Infrared and Optics Division P.O. Box 618 Ann Arbor, Michigan 48107		10. Work Unit No. Task X
		11. Contract or Grant No. NAS5-21783
12. Sponsoring Agency Name and Address National Aeronautics and Space Administration Goddard Space Flight Center Greenbelt, Maryland 20771		13. Type of Report and Period Covered Final Report September 1972-September 1974
		14. Sponsoring Agency Code

15. Supplementary Notes

Mr Edmund F. Szajna (Code 430) monitored this work.

16. Abstract

The objectives of the research were to demonstrate the feasibility of using ERTS multispectral scanner data to map iron compounds on the surfaces of rocks and soils, and to relate the resulting map to geologic features in the Wind River Basin, Wyoming. ERTS data collected in August and October 1972 were processed on digital and special purpose analog recognition computers using ratio enhancement and pattern recognition techniques. Ratios of band-averaged laboratory reflectances of some minerals and rock types known to be in the scene compared favorably with ratios derived from the data by ratio normalization procedures. Although patterns in the recognition map clearly correlated with geologic features, geologic formations could not be separated into compositionally unique groups by this technique.

A single ratio display and density slice of the visible channels of ERTS MSS data, Channel 5/Channel 4 ($R_{5,4}$), separated the Triassic Chugwater Formation (redbeds) from other formations present and may have enhanced iron oxide minerals present at the surface in abundance. This capability may prove important to exploration for those economic deposits characterized by regional iron-oxide alteration. Specific cases illustrating the enhanced features of possible importance in the Wind River Basin are included.

(Abstract continued on next page)

17. Key Words Data processing ERTS-1 Geology Images Iron compounds Mapping Multispectral	 Processing Reflectance Scanners Scientific satellites Spectra Spectral ratioing Temporal ratioing	18 Distribution Statement Initial distribution is indicated at the end of this document.
19. Security Classif. (of this report) UNCLASSIFIED	20. Security Classif. (of this page) UNCLASSIFIED	

PRICES SUBJECT TO CHANGE

1a

(16. Abstract concluded)

Comparison of data sets collected over the same area at two different times of the year (August and October 1973) by digital processing indicated that spectral variation due to environmental factors was reduced by ratio processing. Gray-tones in temporal ratio maps of points not highly vegetated or cloud covered showed decreased dependence on atmospheric and solar illumination over single-channel radiance maps. The temporal ratio technique can be of great importance in applications dependent on either normalization of invariant characteristics or accurate monitoring of changes.

A scheme for comparison of the ERTS response-weighted reflectances is developed using series of numbers to indicate relative reflectances. The resultant ratio code has been computed for the geologic materials in the Earth Resource Spectral Information System Library, housed at the Environmental Research Institute of Michigan. A table of these materials and their ratio codes has been provided.

PREFACE

This report concludes two years of investigations in geologic remote sensing from September, 1972 through September, 1974. All of the work was done at the Environmental Research Institute of Michigan (formerly Willow Run Laboratories of The University of Michigan) under the supervision of Robert K. Vincent, Principal Investigator and Associate Research Geophysicist at ERIM's Infrared and Optics Laboratory (presently of Geospectra Corporation, Ann Arbor, Michigan).

The research described herein was performed under Contract NAS5-21783 as Task X of a project sponsored by the National Aeornautic and Space Administration, Goddard Space Flight Center. Mr. E. Szajna was the Technical Monitor. Interim reports have been published in Proceedings of the Eighth and Ninth International Symposia on Remote Sensing of Environment.

We would like to thank Dr. William C. Kelly and Dr. John A. Dorr of the Department of Geology and Mineralogy, The University of Michigan, for their cooperation in our initial attempts to learn the geology of the region. Roland Kistler of the Environmental Research Institute of Michigan was unendingly resourceful and patient as the analog processor of the major part of the research. Fred Mauk, formerly of Willow Run Laboratories, did the initial computer programming which enabled us to work with laboratory spectral data from the ERSIS data bank. Finally, Fred Thomson of the Environmental Research Institute of Michigan was instrumental in the coordination and completion of the final report.

CONTENTS

Preceding page blank

PAGE 4 INTENTIONALLY BLANK

FIGURES

TABLES

SURFACE COMPOSITIONAL MAPPING BY SPECTRAL RATIOING OF ERTS-1 MSS DATA IN THE WIND RIVER BASIN AND RANGE, WYOMING

1
SUMMARY OF CONCLUSIONS

1. Surface minerals with relatively high reflectance in the red region and low in the green can be mapped using the ERTS-MSS $R_{5,4}$ ratio in arid and semi-arid terrains where vegetation cover is not extensive. Hematite, goethite and limonite, as indicated by their visible characteristic colors of reds and yellows, are good examples of such surface minerals. There is evidence that sedimentary rocks containing only a few percent iron can be mapped, if the iron is well disseminated through the sample. To the extent that surface iron-oxide staining is indicative of mineral or oil deposits, the technique should be useful for prospecting.

2. Analyses of reflectance data collected in the laboratory were used to predict the utility of the ERTS MSS $R_{5,4}$ ratio correctly. These data were also used to establish signatures without in-scene training for supervised automatic pattern recognition of other geologic materials. The procedure was partially successful, but indicated that refinement of procedure would yield better results. Definite promise for recognition of some geologic materials was indicated.

3. Aside from iron-bearing minerals, the geologic targets recognized in supervised automatic recognition were not easily separated into compositionally unique groups, although materials were spectrally distinctive.

4. The success of the $R_{5,4}$ ratio in detecting iron compounds is dependent on strong absorption in the green by the presence of the Fe^{3+} ion with concomitant high reflectivity in red. This spectral information is not necessarily adequately exploited by the wide bands of ERTS. Narrowing of those bands, with selective optimal placement for Fe^{3+} absorption features, should result in increased sensitivity and improve levels of detectability.

5. Corrected ratio images were made independent of environmental changes (atmosphere and solar zenith angle) to within a standard error, $\leq 10\%$ in the case tested.

2
INTRODUCTION

Iron compounds in nature are promising remote-sensing targets because they display prominent spectral features in the visible-reflective infrared wavelength region and are geologically significant. For example, iron oxides are weathering products of mafic minerals,

by-products of hydrothermal alteration, and residual constituents of lateritic soils. Thus, a method for detecting ferric and/or ferrous oxides should contribute to remote sensing efforts concerned with regional geologic mapping, exploration for new mineral resources, and identification of soil types.

Multispectral data processing and automatic recognition procedures using all ERTS-MSS channels were used for this research to allow data preprocessing and use of all spectral data available. The Wind River basin, Wyoming, was chosen as the test site, chiefly because of the known presence of surface iron oxides and the variety of rocks exposed. Laboratory spectra of natural materials were used to predict relative response-weighted reflectance values and for absolute comparison in order to test preprocessing procedures. Several different recognition procedures involving multispectral ratioing with atmospheric correction were used to provide surface composition information for the test area.

The objectives of such research extend beyond the product of this particular data set. If successfully implemented to enhance and/or uniquely recognize concentrations of iron oxides at the surface, the ratio technique should be helpful in the location of uranium, nickel and copper deposits for which iron oxides may act as a surface indicator of ore at depth.

Test data for the Wind River area were collected on 5 August 1972 (E-1013-17294) and 16 October 1972 (E-1085-17300). Processing and analysis extended over a two-year period. Although the scope of this work did not allow iterative procedures which would have given more optimal solutions, some productive efforts have already descended directly from this fundamental study.

3
SPECTRAL RATIO METHODOLOGY

3.1 THEORETICAL DERIVATION

The two major purposes of the spectral ratioing method described below are to suppress spectral effects not related to the chemical or mineralogical composition of geologic targets and to enhance the appearance of selected geologic materials relative to "background" targets, which can include other geologic materials, vegetation and water. The ultimate classification of these materials, using spectral ratioing, is based on the premise that ratio spectra of known materials (training set spectra) are representative of that material throughout the scene. We seek to minimize environmental variations in ratios in order to satisfy this premise, so that accurate classification can be performed.

Consider first the 0.4-2.5 μm spectral region (ERTS-1 includes only the 0.5-1.1 μm region), in which most of the radiation emanating from a target on the earth's surface is reflected solar

radiation. The spectral radiance of a target measured by a multispectral scanner can be expressed as [1, 2]:

$$L'_\lambda = \frac{1}{\pi}\left[\frac{SE_\lambda\,(\text{direct})}{\cos\theta} + E_\lambda(\text{diffuse})\right]\tau(\lambda)\rho(\lambda) + L_\lambda(\text{path}) \tag{1}$$

where L_λ = measured spectral radiance

S = the fraction of the instantaneous field of view covered by shadow

θ = angle between the surface and the line connecting the sun and the earth center

$E_\lambda(\text{direct})$ = direct spectral irradiance of the sun (impinging upon target)

$E_\lambda(\text{diffuse})$ = diffuse spectral irradiance of solar radiation incident on the target from directions other than sun-target direction

$\tau(\lambda)$ = atmospheric transmittance

$\rho(\lambda)$ = spectral reflectance of target

$L_\lambda(\text{path})$ = spectral path radiance (caused by atmospheric scattering)

In Eq. (1) the target is assumed to approximate a quasi-Lambertian reflector, with the angular (slope-angle) dependence of the bidirectional reflectance approximately the same for all wavelengths (i.e., shadow and slope factor (S) is independent of wavelength). The L_λ (path) term represents path radiance caused when light that has not encountered the target is scattered into the beam between target and detector.

Whenever the L_λ(path) term is negligible, as it can be with low altitude aircraft scanner data on a clear, dry day, all of the environmental factors are multiplicative. From satellite altitudes, however, L_λ(path) cannot generally be neglected. To eliminate most of this term under high visibility conditions, one can take the purely empirical approach of <u>dark object subtraction</u>. A dark material in shadow will have signal levels resulting from L_λ(path) and reflected diffuse irradiance, approximating the lowest possible radiance in the scene. For a given spectral channel, the value of the lowest radiance measured within the scene can be subtracted from all other spatial resolution elements to approximately correct for path radiance. If all multispectral channels are assumed to be spectrally narrow in the 0.4-2.5 μm wavelength region, the radiance in the i-th channel can be given by

$$L(i) \approx L_{\lambda_i}\Delta\lambda_i \tag{2}$$

where λ_i is the median wavelength and $\Delta\lambda_i$ is the spectral width (at 50% response points) of the i-th channel. After dark object subtraction, the ratio of the i-th and j-th channels will be approximately equal [1, 3] to:

$$R_{i,j} = \frac{L(i)}{L(j)} \approx \frac{[SE(\text{direct, i}) + E(\text{diffuse, i})]\tau(i)\rho(i)}{[SE(\text{direct, j}) + E(\text{diffuse, j})]\tau(j)\rho(j)} = \frac{E(\text{sun, i})\tau(i)\rho(i)}{E(\text{sun, j})\tau(j)\rho(j)} \tag{3}$$

where E(sun, i) = SE(direct, i) + E(diffuse, i). In Eq. (3) the only terms which should vary widely over most geological test sites are S, cos θ, and $\rho(i)/\rho(j)$, the spectral reflectance ratio of the target. On a clear day of 23 km visibility [1], E(direct, i) is approximately 2.7 times larger than E(diffuse, i) at 0.55 μm. For longer wavelengths, particularly those greater than 0.7 μm, the direct illumination term is much more predominant. The smaller the diffuse illumination term, the less the S and cos θ factors, controlled primarily by topographic variations, affects $R_{i,j}$. When the diffuse term is negligible, as it can be for reflective infrared and sometimes for red spectral channels, the S-factor is essentially cancelled from the $R_{i,j}$ expression in Eq. (3). The $R_{i,j}$ ratio, therefore, is much more independent of topographic variations across the scene than is the single-channel radiance of Eq. (2).

Although $R_{i,j}$ should be relatively invariant with topographic changes across the scene, it still may not be invariant for a given type of target in two data sets collected at different times in different places. For a further suppression of environmental factors [E(sun, i), τ(i) and L(path, i)], one can use the spectral ratio of a known target to normalize to an area within the scene:

$$(R_{i,j})_{ref.} = \frac{E(sun, i)}{E(sun, j)} \frac{\tau(i)}{\tau(j)} \left[\frac{\rho(i)}{\rho(j)}\right]_{ref} \tag{4}$$

Division of Eq. (3) by Eq. (4) yields, after rearrangement, the corrected ratio:

$$R^c_{i,j} \cong \frac{R_{i,j}}{(R_{i,j})_{ref.}} \left(\frac{\rho_i}{\rho_j}\right)_{ref.} \cong \frac{\rho_i}{\rho_j} \tag{5}$$

which is equal to the spectral reflectance ratio of the target, almost independently of environmental factors. The "almost" is included in the foregoing statement because the degree of environmental independence is a function of how well the dark object subtraction succeeds in suppressing the path radiance term. If shadows are present over materials of varying brightness, a more rigorous determination of L_λ(path) can be made, but with greater difficulty [4].

The use of a known reflectance value for calibration of a particular data set is described herein as ratio normalization. This procedure does not help discrimination among targets on a relative basis within a single data set, but it is useful for extending recognition results in time and space. Normalization is necessary for any absolute value determinations using reflectance values from laboratory spectra as training sets. In the future, improved atmospheric models allowing more accurate determination of multiplicative atmospheric terms (see Eq. 4) may alleviate the necessity for in-scene references (see Eq. 5).

3.2 ERTS MULTISPECTRAL RESPONSE-WEIGHTED REFLECTANCES AND RATIO VALUES FOR LABORATORY AND FIELD DATA

Spectral data collected by aircraft or satellite are subject to the bandwidth configuration and response of the detection instrument. Therefore, high resolution spectral data must be averaged before comparison with data collected by a remote sensor. The NASA Earth Resources Spectral Information System (ERSIS) contains laboratory and field measured reflectance spectra for rocks, minerals and soils. The data span the 0.5 - 1.1 μm wavelength range.* A half-sine wave-shaped filter, assumed to approximate the spectral response of the ERTS-MSS channels, was used to average the laboratory and field data to ERTS response-weighted reflectances. Spectral band cutoffs were assumed to be the 50% points of 0.5 μm and 0.6 μm for Channel 4, 0.6 μm and 0.7 μm for Channel 5, 0.7 μm and 0.8 μm for Channel 6, and 0.8 μm and 1.1 μm for Channel 7. Integration of each spectral curve over these intervals results in an average reflectance value per band which should more nearly correspond to that expected from the ERTS scanner.

In accordance with the theory of ratio processing heretofore presented, reflectance ratios for the six nonreciprocal spectral ratios of ERTS channels ($R_{5,4}$, $R_{6,4}$, $R_{6,5}$, $R_{7,4}$, $R_{7,5}$ and $R_{7,6}$, where $R_{i,j}$ means the integrated reflectance of the i-th channel divided by the j-th channel) were calculated for the selected spectra in the data library. These ratio values provide a parameter by which reflectances for any band can be quantitatively and relatively compared and predicted.

3.3. ERTS MULTISPECTRAL RATIO CODES

To facilitate reference to the reflectivities of the variety of materials available, which differ for each sensor configuration, the concept of ratio codes has been developed. A ratio code is a multi-digit number made up of a series of index numbers, one for each ratio represented.. The range over which ratios for the selected rocks, minerals and soils varied for each $R_{i,j}$ was divided into ten intervals, each containing 10% of the spectral curves in the data set. Each of the ten ranges was then assigned a digit from 0 to 9, indicating the decile of the spectral curve population containing the lowest ratio values, etc. Table 1 shows the ratio value ranges for ERTS represented by the ten intervals and the assigned digits for each $R_{i,j}$.

For each of the 379 spectral curves finally selected for the study, a six-digit ratio code was generated, each digit reflecting the relative ratio values of that material for one of the unique ratios of ERTS channels. The digits, left to right, as presented here, correspond to the ratios

*ERSIS is a compilation of laboratory spectral data [5, 6, and 7] housed at the Johnson Space Center in Houston, Texas, and the Environmental Research Institute of Michigan (ERIM) in Ann Arbor, Michigan.

as listed in Table 1. Ratio codes for the selected laboratory reflectance spectra from ERSIS of 59 soil types (133 spectra), 89 minerals (177 spectra), 25 rock types (31 spectra), and 18 types of vegetation (18 spectra) are given in Table 2. The documents from which these spectra originate, listed in Table 3, provide additional descriptive information about the data. Although ratio codes for mineral and rock powders of 0 to 74 μm and 0 to 5 μm grain sizes were cal- in the natural state. Also, many of the laboratory samples were not particularly representative

TABLE 1. RATIO INTERVALS FOR SIX-DIGIT ERTS-MSS RATIO CODE

CODE	1st Digit ($R_{5,4}$)	2nd Digit ($R_{6,4}$)	3rd Digit ($R_{6,5}$)	4th Digit ($R_{7,4}$)	5th Digit ($R_{7,5}$)	6th Digit ($R_{7,6}$)
0	0.398-0.921	0.337-0.938	0.516-0.963	0.296-0.920	0.378-0.946	0.490-0.953
1	0.922-1.014	0.939-1.036	0.964-1.005	0.921-1.058	0.947-1.032	0.954-1.007
2	1.015-1.052	1.037-1.127	1.006-1.036	1.059-1.185	1.033-1.088	1.008-1.036
3	1.053-1.100	1.128-1.214	1.037-1.067	1.186-1.319	1.089-1.140	1.037-1.064
4	1.101-1.168	1.215-1.355	1.068-1.115	1.320-1.523	1.141-1.209	1.065-1.088
5	1.169-1.270	1.356-1.595	1.116-1.171	1.524-1.792	1.210-1.280	1.089-1.132
6	1.271-1.415	1.596-1.845	1.172-1.224	1.293-2.173	1.281-1.402	1.133-1.174
7	1.416-1.629	1.846-2.241	1.225-1.292	2.174-2.645	1.403-1.594	1.175-1.243
8	1.630-1.888	2.242-2.838	1.293-1.364	2.646-3.400	1.595-1.900	1.244-1.365
9	1.889-3.295	2.839-11.747	1.365-11.059	3.401-16.935	1.901-15.944	1.366-3.368

TABLE 2. ERTS-MSS RATIO CODES FOR SELECTED LABORATORY REFLECTANCE SPECTRA FROM THE NASA EARTH RESOURCES SPECTRAL INFORMATION SYSTEM (ERSIS)

Note: * denotes the highest value for that ratio of any spectrum in this data collection; the code for that ratio is a "9".

SAMPLE NAME AND DESCRIPTION			ERSIS DOCUMENT NUMBER	ERTS-MSS RATIO CODE
SOILS				
CLAY				
CLAY, ALONSO TYPE	DRY	PUERTO RICO	B00830203	778776
CLAY, ALONSO TYPE	WET	PUERTO RICO	B00830205	989886
CLAY, MATANZAS TYPE	DRY	CUBA	B00830117	999987
CLAY, MATANZAS TYPE	WET	CUBA	B00830118	999986
CLAY, ORIENTE TYPE	DRY	CUBA	B00830101	333333
CLAY, ORIENTE TYPE	WET	CUBA	B00830102	555444
CLAY, ORMAN TYPE	DRY	N. CAROLINA	B00830097	545578
CLAY, ORMAN TYPE	WET	N. CAROLINA	B00830099	556678
CLAY, QUIBDO GRAVELLY	DRY		B00830001	764643
CLAY, QUIBDO GRAVELLY	WET		B00830003	986864
LOAM (UNSPECIFIED)				
LOAM, AKRON TYPE	DRY	ALABAMA	B00830075	997975
LOAM, AKRON TYPE	WET	ALABAMA	B00830076	998975
LOAM, ALBION TYPE	DRY	KANSAS	B00830082	778889
LOAM, ALBION TYPE	WET	KANSAS	B00830084	668899
LOAM, BLAKELY TYPE	DRY	GEORGIA	B00830062	987877
LOAM, BLAKELY TYPE	WET	GEORGIA	B00830064	986877
LOAM, CLARION	DRY	IOWA	B00830017	668899
LOAM, CLARION	WET	IOWA	B00830019	569899
LOAM, COLTS NECK TYPE	DRY	NEW JERSEY	B00830049	877651
LOAM, COLTS NECK TYPE	WET	NEW JERSEY	B00830051	877630
LOAM, COLTS NECK TYPE	DRY	NEW JERSEY	B00830059	987862
LOAM, COLTS NECK TYPE	WET	NEW JERSEY	B00830060	988751
LOAM, COLTS NECK TYPE	DRY	NEW JERSEY	B00830141	999874
LOAM, COLTS NECK TYPE	WET	NEW JERSEY	B00830142	988761
LOAM, GREENVILLE TYPE	DRY	LOUISIANA	B00830159	998961
LOAM, GREENVILLE TYPE	WET	LOUISIANA	B00830161	998974
LOAM, HAMAKUA, HEAVY TYPE	DRY	HAWAII	B00830079	876763
LOAM, HAMAKUA, HEAVY TYPE	WET	HAWAII	B00830080	777651
LOAM, ONOMEA TYPE	DRY	HAWAII	B00830131	444443
LOAM, ONOMEA TYPE	WET	HAWAII	B00830132	532446
LOAM, WELD TYPE	DRY	COLORADO	B00830133	667788
LOAM, WELD TYPE	WET	COLORADO	B00830134	778788

TABLE 2 (cont.)

IPLE NAME AND DESCRIPTION			ERSIS DOCUMENT NUMBER	ERTS-MSS RATIO CODE
_OAM (CLAY TYPE)				
LOAM, AIKEN CLAY	DRY	OREGON	B00830029	776652
LOAM, AIKEN CLAY	WET	OREGON	B00830031	877651
LOAM, BLAKELY CLAY TYPE	DRY	GEORGIA	B00830183	888887
LOAM, BLAKELY CLAY TYPE	WET	GEORGIA	B00830185	877778
LOAM, CLAREVILLE CLAY	DRY	TEXAS	B00830105	544455
LOAM, CLAREVILLE CLAY	WET	TEXAS	B00830106	766677
LOAM, DUBLIN CLAY	DRY	CALIFORNIA	B00830125	456689
LOAM, DUBLIN CLAY	WET	CALIFORNIA	B00830126	334579
LOAM, MOAULA LIGHT CLAY	DRY	HAWAII	B00830037	887764
LOAM, MOAULA LIGHT CLAY	WET	HAWAII	B00830039	999985
LOAM, MOAULA LIGHT CLAY	DRY	HAWAII	B00830127	988875
LOAM, MOAULA LIGHT CLAY	WET	HAWAII	B00830128	999884
LOAM, NAALEHU HEAVY CLAY	DRY	HAWAII	B00830061	888775
LOAM, NAALEHU HEAVY CLAY	WET	HAWAII	B00830063	889875
LOAM, NAALEHU HEAVY CLAY	DRY	HAWAII	B00830151	887764
LOAM, NAALEHU HEAVY CLAY	WET	HAWAII	B00830153	999986
LOAM, OOKALA CLAY	DRY	HAWAII	B00830109	888761
LOAM, OOKALA CLAY	WET	HAWAII	B00830110	776642
LOAM, OOKALA CLAY	DRY	HAWAII	B00830113	887763
LOAM, OOKALA CLAY	WET	HAWAII	B00830114	777663
LOAM, PIERRE CLAY	DRY	WYOMING	B00830071	545567
LOAM, PIERRE CLAY	WET	WYOMING	B00830072	554567
_OAM (SILT TYPE)				
LOAM, AGUAN SILT	DRY	HONDURAS	B00830025	656566
LOAM, AGUAN SILT	WET	HONDURAS	B00830027	557676
LOAM, ALAMANCE SILT	DRY	S. CAROLINA	B00830123	555455
LOAM, ALAMANCE SILT	WET	S. CAROLINA	B00830124	766676
LOAM, DECATUR SILT	DRY	TENNESSEE	B00830089	877777
LOAM, DECATUR SILT	WET	TENNESSEE	B00830091	877888
LOAM, GUTHRIE SILT	DRY	KENTUCKY	B00830149	656566
LOAM, GUTHRIE SILT	WET	KENTUCKY	B00830150	779788
LOAM, HERRADURA PURE SILT	DRY	CUBA	B00830021	764532
LOAM, HERRADURA PURE SILT	WET	CUBA	B00830023	875620
LOAM, MARSHALL SILT	DRY	IOWA	B00830119	667899
LOAM, MARSHALL SILT	WET	IOWA	B00830120	668899
LOAM, MAURY SILT	DRY	TENNESSSE	B00830081	878777
LOAM, MAURY SILT	WET	TENNESSSE	B00830083	988888
LOAM, PENN SILT	DRY	N. CAROLINA	B00830098	778888
LOAM, PENN SILT	WET	N. CAROLINA	B00830100	778899
LOAM, TILSIT SILT	DRY	INDIANA	B00830143	655544
LOAM, TILSIT SILT	WET	INDIANA	B00830145	765665
LOAM, ZANESVILLE SILT	DRY	INDIANA	B00830041	654555
LOAM, ZANESVILLE SILT	WET	INDIANA	B00830043.	654555

TABLE 2 (cont.)

SAMPLE NAME AND DESCRIPTION			ERSIS DOCUMENT NUMBER	ERTS-MSS RATIO CODE
LOAM (SANDY TYPE)				
LOAM, BARNES FINE SANDY	DRY	S. DAKOTA	B00830087	668899
LOAM, BARNES FINE SANDY	WET	S. DAKOTA	B00830088	568899
LOAM, BLACK VOLCANIC SANDY	DRY	GUATEMALA	B00830191	778788
LOAM, BLACK VOLCANIC SANDY	WET	GUATEMALA	B00830193	668789
LOAM, COLLINGTON TYPE	WET	MARYLAND	B01339007	555565
LOAM, GOOCH FINE SANDY	DRY	OREGON	B00830144	545455
LOAM, GOOCH FINE SANDY	WET	OREGON	B00830146	666665
LOAM, GRADY SANDY	DRY	GEORGIA	B00830121	456689
LOAM, GRADY SANDY	WET	GEORGIA	B00830122	557799
LOAM, GREENVILLE SANDY	DRY	GEORGIA	B00830057	876631
LOAM, GREENVILLE SANDY	WET	GEORGIA	B00830058	987620
LOAM, HALL VERY FINE SANDY	DRY	NEBRASKA	B00830066	557789
LOAM, HALL VERY FINE SANDY	WET	NEBRASKA	B00830068	668899
LOAM, ORANGEBURG TYPE	DRY	LOUISIANA	B00830147	987865
LOAM, ORANGEBURG TYPE	WET	LOUISIANA	B00830148	998875
LOAM, PUTNAM FINE SANDY	DRY	OKLAHOMA	B00830085	777889
LOAM, PUTNAM FINE SANDY	WET	OKLAHOMA	B00830086	889999
LOAM, RUSTON SANDY TYPE	DRY	GEORGIA	B00830053	996863
LOAM, RUSTON SANDY TYPE	WET	GEORGIA	B00830055	998976
LOAM, RUSTON SANDY	DRY	GEORGIA	B00830093	986752
LOAM, RUSTON SANDY	WET	GEORGIA	B00830095	887740
LOAM, RUSTON SANDY	DRY	GEORGIA	B00830129	654533
LOAM, RUSTON SANDY	WET	GEORGIA	B00830130	875643
LOAM, SANTA BARBARA TYPE	DRY	CUBA	B00830069	765531
LOAM, SANTA BARBARA TYPE	WET	CUBA	B00830070	876520
LOAM, SANTA BARBARA TYPE	DRY	CUBA	B00830163	765642
LOAM, SANTA BARBARA TYPE	WET	CUBA	B00830165	886752
LOAM, TIFTON SANDY TYPE	DRY	GEORGIA	B00830077	765542
LOAM, TIFTON SANDY TYPE	WET	GEORGIA	B00830078	876641
LOAM, TILLMAN FINE SANDY	DRY	OKLAHOMA	B00830073	999988
LOAM, TILLMAN FINE SANDY	WET	OKLAHOMA	B00830074	999987
LOAM, VERNON VERY FINE	DRY	TEXAS	B00830103	988888
LOAM, VERNON VERY FINE	WET	TEXAS	B00830104	998988
LOAM, WELD FINE SANDY	DRY	COLORADO	B00830137	777788
LOAM, WELD FINE SANDY	WET	COLORADO	B00830138	778788
LOAM, JOPLIN STONY	DRY	MONTANA	B00830090	766678
LOAM, JOPLIN STONY	WET	MONTANA	B00830092	778787

TABLE 2 (cont.)

SAMPLE NAME AND DESCRIPTION				ERTS DOCUMENT NUMBER	ERTS-MSS RATIO CODE
SAND					
SAND, COLTS NECK LOAMY		DRY	NEW JERSEY	B00830111	876641
SAND, COLTS NECK LOAMY		WET	NEW JERSEY	B00830112	887640
SAND, ORANGEBURG		DRY	N. CAROLINA	B00830115	997863
SAND, ORANGEBURG		WET	N. CAROLINA	B00830116	997851
SAND, RUBICON		DRY	MICHIGAN	B00830005	656677
SAND, RUBICON		WET	MICHIGAN	B00830007	778788
SAND, RUSTON FINE TYPE		DRY	N. CAROLINA	B00830139	875641
SAND, RUSTON FINE TYPE		WET	N. CAROLINA	B00830140	986630
SAND, WINDTHORST TYPE		DRY	OKLAHOMA	B00830107	997977
SAND, WINDTHORST TYPE		WET	OKLAHOMA	B00830108	998988
SAND, WINDTHORST TYPE		DRY	OKLAHOMA	B00830199	777778
SAND, WINDTHORST TYPE		WET	OKLAHOMA	B00830201	888999
SAND, LIGHT TAN WITH GRASS			FLORIDA	A02010101	888888
SAND, LIGHT TAN WITH GRASS			FLORIDA	A02010201	889999
SAND, COARSE GREY			FLORIDA	A02012101	555567
SAND, GRAY WASHED PIT			MICHIGAN	A02013101	444455
SAND, TEXAS DUNE		DRY		B00830033	765665
SAND, TEXAS DUNE		WET		B00830035	876776
WHITE SAND	DRY		MARYLAND	B01339003	544445
WHITE SAND	WET		MARYLAND	B01339005	544445
YELLOW SAND	DRY		MARYLAND	B01339004	654544
YELLOW SAND	WET		MARYLAND	B01339006	765542
MINERALS					
SILICATES					
AMPH.,TREMOLITE	74- 250	MICR	NEW YORK	B09000003	111100
AMPH.,TREMOLITE	250-1200	MICR	NEW YORK	B09000004	211000
AMPH.,TREMOLITE	74- 250	MICR	NEW YORK	B09000007	100001
AMPH.,TREMOLITE	250-1200	MICR	NEW YORK	B09000008	211000
AMPH.,ACTINOLITE	74- 250	MICR	VERMONT	B09000011	003021
AMPH. ACTINOLITE	250-1200	MICR	VERMONT	B09000012	112111
AMPH. ACTINOLITE	74- 250	MICR	CALIFORNIA	B09000015	001011
AMPH. ACTINOLITE	250-1200	MICR	CALIFORNIA	B09000016	000001
AMPH. HORNBLENDE	74- 250	MICR	NEW YORK	B09000019	236478
AMPH. HORNBLENDE	250-1200	MICR	NEW YORK	B09000020	111125
AMPH. HORNBLENDE	74- 250	MICR	NEW YORK	B09000023	001124
AMPH. HORNBLENDE	250-1200	MICR	NEW YORK	B09000024	112122
AMPH. HORNBLENDE	74- 250	MICR	NEW YORK	B09000027	333356
AMPH. HORNBLENDE	250-1200	MICR	NEW YORK	B09000028	310113
ANDALUSITE	74- 250	MICR	AUSTRALIA	B09000031	544556
ANDALUSITE	250-1200	MICR	AUSTRALIA	B09000032	543456
ANORTHOCLASE	74- 250	MICR	LARVIK, NORWAY	B09000035	444466
ANORTHOCLASE	250-1200	MICR	LARVIK, NORWAY	B09000036	434456

TABLE 2 (cont.)

SAMPLE NAME AND DESCRIPTION				ERSIS DOCUMENT NUMBER	ERTS-MSS RATIO CODE
BERYL	74- 250	MICR	MAINE	B09000039	100007
BERYL	250-1200	MICR	MAINE	B09000040	100006
BIOTITE	250-1200	MICR	ONT., CANADA	B09000043	221235
CHABAZITE	74- 250	MICR	COLORADO	B09000045	433334
CHLORITE	74- 250	MICR	COLORADO	B09000048	333356
CHLORITE	74- 250	MICR	CALIFORNIA	B09000052	000006
CHLORITE	250-1200	MICR	CALIFORNIA	B09000050	000005
DANBURITE	74- 250	MICR	NEW YORK	B09000055	310112
DANBURITE	250-1200	MICR	NEW YORK	B09000056	431323
DUMORTIERITE	74- 250	MICR	NEVADA	B09000059	666667
DUMORTIERITE	250-1200	MICR	NEVADA	B09000060	668788
KAOLINITE	74- 250	MICR	NEW MEXICO	B09000062	322223
KAOLINITE	250-1200	MICR	NEW MEXICO	B09000063	322223
KAOLINITE	74- 250	MICR	GEORGIA	B09000070	333334
KAOLINITE	250-1200	MICR	GEORGIA	B09000071	434344
MONTMORILLONITE	74- 250	MICR	MISSISSIPPI	B09000073	655531
MONTMORILLONITE	250-1200	MICR	MISSISSIPPI	B09000074	665531
MONTMORILLONITE	74- 250	MICR	MISSISSIPPI	B09000077	653422
MONTMORILLONITE	250-1200	MICR	MISSISSIPPI	B09000078	541200
MUSCOVITE	74- 250	MICR	ONT., CANADA	B09000081	223235
OLIVINE-FORSTERITE	74- 250	MICR	CALIFORNIA	B09000089	222211
OLIVINE-FORSTERITE	250-1200	MICR	CALIFORNIA	B09000090	544321
OLIVINE-FAYALITE	74- 250	MICR	N. CAROLINA	B09000093	100000
OLIVINE-FAYALITE	250-1200	MICR	N. CAROLINA	B09000094	100000
ORTHOCLASE	74- 250	MICR	NEW HAMPSHIRE	B09000102	333333
ORTHOCLASE	250-1200	MICR	NEW HAMPSHIRE	B09000103	433344
PLAG. ALBITE	74- 250	MICR	VIRGINIA	B09000106	223234
PLAG. ALBITE	250-1200	MICR	VIRGINIA	B09000107	222233
PLAG. OLIGOCLASE	74- 250	MICR	NORWAY	B09000110	222223
PLAG. OLIGOCLASE	250-1200	MICR	NORWAY	B09000111	322223
PLAG. ANDESINE	74- 250	MICR	MONTANA	B09000114	443444
PLAG. ANDESINE	250-1200	MICR	MONTANA	B09000115	432335
PLAG. LABRADORITE	74- 250	MICR	NEW YORK	B09000118	111223
PLAG. LABRADORITE	250-1200	MICR	NEW YORK	B09000119	111113
PLAG. BYTOWNITE	74- 250	MICR	MINNESOTA	B09000122	110113
PLAG. BYTOWNITE	250-1200	MICR	MINNESOTA	B09000123	100012
PYRX. AUGITE	74- 250	MICR	CANADA	B09000126	100013
PYRX. AUGITE	250-1200	MICR	CANADA	B09000127	000014
PYRX. DIOPSIDE	74- 250	MICR	NEW YORK	B09000130	000000
PYRX. DIOPSIDE	250-1200	MICR	NEW YORK	B09000131	000000
PYRX. HEDENBERGITE	74- 250	MICR	MONTANA	B09000134	422334
PYRX. HEDENBERGITE	250-1200	MICR	MONTANA	B09000135	542322
PYRX. HYPERSTHENE	74- 250	MICR	CANADA	B09000137	667530
PYRX. HYPERSTHENE	250-1200	MICR	CANADA	B09000138	545100
PYRX., BRONZITE	74- 250	MICR	N. CAROLINA	B09000141	410000

TABLE 2 (cont.)

SAMPLE NAME AND DESCRIPTION				ERSIS DOCUMENT NUMBER	ERTS-MSS RATIO CODE
PYRX.,BRONZITE	250-1200	MICR	N. CAROLINA	B09000142	630000
QUARTZ	250-1200	MICR		B09000145	211223
QUARTZ, MILKY	149- 250	MICR		B09000146	333334
QUARTZ, MILKY	250- 420	MICR		B09000147	433344
SERPENTINE	250-1200	MICR	MISSOURI	B09000155	000001
TALC	74- 250	MICR	N. CAROLINA	B09000066	311112
TALC	250-1200	MICR	N. CAROLINA	B09000067	100000
OXIDES AND HYDROXIDES					
BRUCITE	74- 250	MICR	NEVADA	B09005003	322212
BRUCITE	250-1200	MICR	NEVADA	B09005004	321100
CASSITERITE	250-1200	MICR	NIGERIA	B09005007	667552
CASSITERITE	74- 250	MICR	NIGERIA	B09005008	543321
CHRYSOBERYL	74- 250	MICR	S. DAKOTA	B09005011	334345
CHRYSOBERYL	250-1200	MICR	S. DAKOTA	B09005012	334456
CORUNDUM	74- 250	MICR	TRANSVALL,AFRICA	B09005017	334467
CORUNDUM	250-1200	MICR	TRANSVALL,AFRICA	B09005018	445578
CUPRITE	74- 250	MICR	MONTANA	B09005019	887889
CUPRITE	250-1200	MICR	MONTANA	B09005020	888888
DIASPORE	74- 250	MICR	MISSOURI	B09005024	456678
DIASPORE	250-1200	MICR	MISSOURI	B09005025	555567
GIBBSITE	74- 250	MICR	BRAZIL	B09005028	544455
GIBBSITE	250-1200	MICR	BRAZIL	B09005029	555555
GOETHITE	74- 250	MICR	MINNESOTA	B09005032	642311
GOETHITE	250-1200	MICR	MINNESOTA	B09005033	640312
HEMATITE	74- 250	MICR	MINNESOTA	B09005036	888887
ILMENITE	74- 250	MICR	NORWAY	B09005039	345466
LIMONITE	74- 250	MICR		B09004003	776520
LIMONITE (SAWED PLATE)				B09004004	665420
LIMONITE	250-1200	MICR		B09004005	766542
LIMONITE	250-1200	MICR	ALABAMA	B09005042	889650
MAGNETITE	74- 250	MICR	COLORADO	B09005045	320225
MAGNETITE	74- 250	MICR	MICHIGAN	B09005048	200102
PSILOMELANE	74- 250	MICR	NEW MEXICO	B09005050	122234
PSILOMELANE	250-1200	MICR	NEW MEXICO	B09005051	001124
PYROLUSITE	74- 250	MICR	COLORADO	B09005053	322457
PYROLUSITE	250-1200	MICR	COLORADO	B09005054	334467
PYROLUSITE	74- 250	MICR	BRAZIL	B09005057	556678
PYROLUSITE	250-1200	MICR	BRAZIL	B09005058	766789
RUTILE	74- 250	MICR	MEXICO	B09005060	889889
RUTILE	250-1200	MICR	MEXICO	B09005061	789999
RUTILE	74- 250	MICR	GEORGIA	B09005063	779899
RUTILE	250-1200	MICR	GEORGIA	B09005064	778788
ZINCITE	74- 250	MICR	NEW JERSEY	B09005067	887776
ZINCITE	250-1200	MICR	NEW JERSEY	B09005068	641447

TABLE 2 (cont.)

SAMPLE NAME AND DESCRIPTION				ERSIS DOCUMENT NUMBER	ERTS-MSS RATIO CODE
CARBONATES					
AZURITE	74- 250	MICR	ARIZONA	B09008003	000169
AZURITE	250-1200	MICR	ARIZONA	B09008004	000049
CALCITE	74- 250	MICR	MEXICO	B09008006	212223
CALCITE	250-1200	MICR	MEXICO	B09008008	211224
CALCITE	74- 250	MICR	KANSAS	B09008010	212122
CALCITE	250-1200	MICR	KANSAS	B09008012	111111
CALCIUM CARBONATE, GRANULAR				B04804001	111122
DOLOMITE	74- 250	MICR	MASSACHUSETTS	B09008015	111112
DOLOMITE	250-1200	MICR	MASSACHUSETTS	B09008016	111111
DOLOMITE	74- 250	MICR	NEW YORK	B09008019	212222
DOLOMITE	250-1200	MICR	NEW YORK	B09008020	222111
MAGNESITE	250-1200	MICR	CALIFORNIA	B09008023	222234
MAGNESITE	74- 250	MICR	CALIFORNIA	B09008024	222223
MAGNESITE	74- 250	MICR	NORWAY	B09008026	211100
MAGNESITE	250-1200	MICR	NORWAY	B09008027	221000
MALACHITE	74- 250	MICR	ARIZONA	B09008030	000006
MALACHITE	250-1200	MICR	ARIZONA	B09008031	000008
RHODOCHROSITE	74- 250	MICR	ARGENTINA	B09008033	653300
RHODOCHROSITE	250-1200	MICR	ARGENTINA	B09008034	752300
SIDERITE	74- 250	MICR	CONNECTICUT	B09008036	655100
SIDERITE	250-1200	MICR	CONNECTICUT	B09008037	666410
SMITHSONITE	74- 250	MICR	NEW MEXICO	B09008039	100000
SMITHSONITE	250-1200	MICR	NEW MEXICO	B09008040	000000
STRONTIANITE	74- 250	MICR	WESTPHALIA	B09008041	333334
STRONTIANITE	250-1200	MICR	WESTPHALIA	B09008042	333334
WITHERITE	74- 250	MICR		B09008044	222223
WITHERITE	250-1200	MICR		B09008045	222234
SULPHUR, SULFATES, AND SULFIDES					
ALUNITE	74- 250	MICR	UTAH	B09009003	554444
ALUNITE	250-1200	MICR	UTAH	B09009004	765653
ANNABERGITE	74- 250	MICR	NEVADA	B30000004	001247
ANNABERGITE	250-1200	MICR	NEVADA	B30000005	000148
ARSENOPYRITE	74- 250	MICR	UTAH	B09009007	333333
ARSENOPYRITE	250-1200	MICR	UTAH	B09009008	544432
BARITE	74- 250	MICR	COLORADO	B09009011	655566
BARITE	250-1200	MICR	COLORADO	B09009012	655666
CELESTITE	74- 250	MICR	MEXICO	B09009015	345465
CELESTITE	250-1200	MICR	MEXICO	B09009016	457577
CHALCOCITE	74- 250	MICR	MONTANA	B09009020	100002

TABLE 2 (cont.)

SAMPLE NAME AND DESCRIPTION				ERSIS DOCUMENT NUMBER	ERTS-MSS RATIO CODE
CHALCOCITE	250-1200	MICR	MONTANA	B09009021	000002
CHALCOPYRITE	74- 250	MICR	CANADA	B09009024	445331
CHALCOPYRITE	250-1200	MICR	CANADA	B09009025	001012
CINNABAR	74- 250	MICR	NEVADA	B09009027	995955
CINNABAR	250-1200	MICR	NEVADA	B09009028	993846
COBALTITE	74- 250	MICR	CANADA	B09009031	211224
COBALTITE	250-1200	MICR	CANADA	B09009032	432334
ENARGITE	74- 250	MICR	PERU	B09009035	224468
ENARGITE	250-1200	MICR	PERU	B09009036	112357
GALENA	74- 250	MICR	KANSAS	B09009039	000012
GYPSUM	74- 250	MICR	ITALY	B09009042	222222
GYPSUM	250-1200	MICR	ITALY	B09009043	222112
GYPSUM	74- 250	MICR	UTAH	B09009046	111112
GYPSUM	250-1200	MICR	UTAH	B09009047	212112
GYPSUM	74- 250	MICR	NEW YORK	B09009050	223223
GYPSUM	250-1200	MICR	NEW YORK	B09009051	223223
GYPSUM	74- 250	MICR	NEW YORK	B09009052	333333
GYPSUM DUNE SAND			NEW MEXICO	B30010001	112122
JAMESONITE	74- 250	MICR	BOLIVIA	B09009058	555555
JAMESONITE	250-1200	MICR	BOLIVIA	B09009059	555567
JAROSITE (ROUGH SURFACE)			NEVADA	B09009060	654410
MARCASITE	74- 250	MICR	OKLAHOMA	B09009063	123233
MARCASITE	250-1200	MICR	OKLAHOMA	B09009064	110113
MOLYBDENITE	74- 250	MICR	UTAH	B09009066	346699
MOLYBDENITE	250-1200	MICR	UTAH	B09009067	247799
NICCOLITE	74- 250	MICR	CANADA	B09009069	333456
NICCOLITE	250-1200	MICR	CANADA	B09009070	433456
PROUSTITE	74- 250	MICR	COLORADO	B09009072	469799
PROUSTITE	250-1200	MICR	COLORADO	B09009073	469799
PYRARGYRITE	74- 250	MICR	NEVADA	B09009075	223357
PYRARGYRITE	250-1200	MICR	NEVADA	B09009076	222346
PYRITE	74- 250	MICR	COLORADO	B09009079	532210
PYRITE	250-1200	MICR	COLORADO	B09009080	333211
PYRRHOTITE	74- 250	MICR	CANADA	B09009083	764656
PYRRHOTITE	250-1200	MICR	CANADA	B09009084	876777
REALGAR	74- 250	MICR	NEVADA	B09009086	*96977
REALGAR	250-1200	MICR	NEVADA	B09009087	996977
SPHALERITE	74- 250	MICR	COLORADO	B09009089	333356
STIBNITE	74- 250	MICR	MEXICO	B09009092	279999
STIBNITE	250-1200	MICR	MEXICO	B09009093	48999*
SULPHUR	74- 250	MICR	NEVADA	B09009096	444455
SULPHUR	250-1200	MICR	NEVADA	B09009097	445466
THENARDITE	74- 250	MICR	CALIFORNIA	B09009101	323333
THENARDITE	250-1200	MICR	CALIFORNIA	B09009102	334344

TABLE 2 (cont.).

SAMPLE NAME AND DESCRIPTION			ERSIS DOCUMENT NUMBER	ERTS-MSS RATIO CODE
HALIDES				
ATACAMITE,NATURAL SURFACE		MEXICO	B30000001	000024
SYLVITE	74- 250 MICR	NEW MEXICO	B30000003	421110
SYLVITE	250-1200 MICR	NEW MEXICO	B30000002	432222
BORATES,PHOSPHATES, AND VANADATES				
COLEMANITE (BOR.)	74- 250 MICR	CALIFORNIA	B30000009	223233
COLEMANITE (BOR.)	250-1200 MICR	CALIFORNIA	B30000010	222212
ULEXITE (BOR.)	74- 250 MICR	CALIFORNIA	B30000011	211112
VIVIANITE (PHOS.)	74- 250 MICR	NEW JERSEY	B30000007	431324
VIVIANITE (PHOS.)	250-1200 MICR	NEW JERSEY	B30000008	544433
CARNOTITE (VAN.)		COLORADO	B30000006	444456
ROCKS				
IGNEOUS				
HORNBL. ANDESITE	420-500 MICR	CALIFORNIA	B09012026	321100
PORPHYRY ANDESITE	420-500 MICR	COLORADO	B09012021	432211
BASALT	420-500 MICR	OREGON	B09012028	001011
BASALT			B14004091	002011
BASALT, MALPAIS FLOW		NEW MEXICO	B30010003	445568
BASALTIC LAVA, BROKEN SURFACE			B09004013	113245
BASALTIC LAVA, IRON OXIDE STAINED			B09004010	224334
BASALTIC LAVA			B14004084	421100
BASALT LAVA, ALTERED SURFACE			A01697001	100000
HORNBL. DIORITE	420-500 MICR	MASSACHUSETTS	B09012016	111111
PORPHYRY DIORITE	420-500 MICR	CANADA	B09012018	222111
BYTOWNITE GABBRO	420-500 MICR	MINNESOTA	B09012024	111112
BIOTITE GRANITE	420-500 MICR	RHODE ISLAND	B09012029	444445
HORNBL. GRANITE	420-500 MICR	MASSACHUSETTS	B09012020	222245
POTASH GRANITE			B14004095	114245
GRANODIORITE	420-500 MICR	MINN.	B09012017	433333
OBSIDIAN	420-500 MICR	OREGON	B09012022	111000
MICA-AUG. PERID.	420-500 MICR	ARKANSAS	B09012023	111111
PERID.-SERP.	420-500 MICR	NEW YORK	B09012030	111101
PUMICE			B09004011	654556
GREY RHYOLITE	420-500 MICR	COLORADO	B09012019	323233
PINK RHYOLITE	420-500 MICR	COLORADO	B09012027	544444

TABLE 2 (Concluded)

SAMPLE NAME AND DESCRIPTION		ERSIS DOCUMENT NUMBER	ERTS-MSS RATIO CODE
SEDIMENTARY AND METAMORHIC			
CHERT		A00263001	444456
FLINT		B14004096	667677
GREENSTONE,ALTERED BASALT		A00261001	000001
LIMESTONE		B14004087	446578
MARBLE		B14004094	113121
PLAYA CRUST	NEW MEXICO	B30010002	556566
SANDSTONE, RED		B14004090	000015
SANDSTONE, YELLOW		B14004088	555566
SHALE		B14004086	111224
VEGETATION			
GRASS AND MOSS			
CLOVER		B09004008	099999
SWAMP GRASS (GREEN)		B01176007	099997
GRASS (COARSE)		B09004007	099999
GRASS (DEAD)		B01176048	667799
MOSS (HEALTHY, NON-FRUITING)		B20000391	3****9
SPHAGNUM MOSS		B03333001	089897
STRAW		B01176046	767788
CONIFEROUS TREES			
PINE NEEDLES		B09004009	099996
BLACK PINE (NEEDLES)		B01176006	099997
PONDEROSE PINE (HEALTHY NEEDLES)		B03333012	099997
WHITE PINE (NEEDLES)		B03070003	099998
RED PINE (NEEDLES)		B03559007	099997
JACK PINE (BARK)		B01818027	889999
DECIDUOUS TREES			
AMERICAN ASH (NEW LEAF)		B00829128	099998
DOGWOOD (NEW LEAF)		B00829152	099997
RED.MAPLE (NEW LEAF)		B00829138	099998
OAK (GREEN. LEAF)		B01176003	099998
SYCAMORE (GREEN LEAF, UPPER SURFACE)		B04803003	199997

TABLE 3. SOURCE DOCUMENTS FOR ERSIS LABORATORY SPECTRA

DOCUMENT NUMBER	REFERENCE
B00829	Hopkins; Reflectance Curves of Various Leaves, USAERDL, Ft. Belvoir, Virginia, ca. 1955 (unpublished).
B00830	Hopkins; Reflectance Curves of Various Soils, USAERDL, Ft. Belvoir, Virginia, ca. 1955 (unpublished)
B01176	Wright: Spectral Reflectance Characteristics of Camouflage Greens Versus Camouflage Detection, IRMA III Report No. 1281, USAERDL, Ft. Belvoir, Virginia, March 1953.
B01339	Haas, et. al.: Spectrophotometric and Colorimetric Study of Color Transparencies of Some Natural Objects, Report No. 4794, NBS, Washington, D.C., March 1957.
B01818	Kronstein: Research, Studies, and Investigations on Spectral Reflectances and Absorption Characteristics of Camouflage Paint Materials and Natural Objects, Final Report, Contract DA-44-009 ENG-1447, New York University, New York, March 1955.
B03070	Gates, et al.: "Spectral Properties of Plants," Appl. Opt., Vol. 4, No. 1, 1965.
B03333	Infrared Optical Measurements, Report No. 8626, NBS, Washington, D.C., December 1964.
B03559	Barbrow; Calibration on the Spectral Directional Reflectance of Six Samples of Red Pine Needles, NBS, Test No. G-35201-1, Agricultural Research Center, Belleville, Maryland, November 1964 (unpublished).
B04803	Cooper, Derksen: Spectral Reflectance and Transmittance of Forest Fuel Materials (Final Report), Material Laboratory, New York Naval Shipyard, Brooklyn, New York, March 1952.
B04804	Hovis: "Infrared Reflectivity of Some Common Minerals," Applied Optics, Vol. 5, 1966.
B09000	Hunt, Salisbury: "Visible and Near-Infrared Spectra of Minerals and Rocks: I. Silicate Minerals," Mod. Geol., Vol. I, 1970, pp. 283-300.

TABLE 3 (cont.)

DOCUMENT NUMBER	REFERENCE
B00830	Hopkins: Reflectance Curves of Various Soils, USAERDL, Ft. Belvoir, Virginia, ca. 1955 (unpublished).
B09005	Hunt, Salisbury: "Visible and Near-Infrared Spectra of Minerals and Rocks: III. Oxides and Hydroxides," Mod. Geol., Vol. II, 1971, pp. 195-205.
B09008	Hunt, Salisbury: "Visible and Near-Infrared Spectra of Minerals and Rocks: II. Carbonates," Mod. Geol., Vol. II, 1971, pp. 23-30.
B09009	Hunt, Salisbury: "Visible and Near-Infrared Spectra of Minerals and Rocks: IV. Sulphides and Sulphates," accepted by Mod. Geol. for 1971.
B09012	Ross, Adler, Hunt: "A Statistical Analysis of the Reflectance of Igneous Rocks from 0.2 to 2.65 Microns," Icarus, Vol. 11, 1969, pp. 46-54.
B14004	Williamson: Night Reconnaissance Subsystem (U), (Final Technical Documentary Report), Martin-Marietta Corp., Orlando, Florida, November 1964, AD 355 324 (CONFIDENTIAL)
B20000	Reflectance of Target and Background Materials, unpublished data from the Air Force Target Signature Measurement Program, Willow Run Laboratories of the Institute of Science and Technology, The University of Michigan, Ann Arbor, 1967.
B30000	Hunt, Salisbury, Lenhoff: "Visible and Near-Infrared Spectra of Minerals and Rocks: V. Halides, Phosphates, Arsenates, Vanadates and Borates," Mod. Geol., Vol. III, 1972, pp. 121-132.
B30010	Lindberg, Smith: "Reflectance Spectra of Gypsum Sand from the White Sands National Monument and Basalt from a Nearby Lava Flow," The American Mineralogist, Vol. 58, 1973, pp. 1062-1064.
A00263	Measured at Environmental Research Institute of Michigan.
A00261	Measured at Environmental Research Institute of Michigan.
A01697	Measured at Environmental Research Institute of Michigan.

TABLE 3 (Concluded)

DOCUMENT NUMBER	REFERENCE
A02010	Measured at Environmental Research Institute of Michigan.
A02012	Measured at Environmental Research Institute of Michigan.
A02013	Measured at Environmental Research Institute of Michigan.

of surface materials, in that they were unweathered samples. It should be noted that these ratio codes supersede the ratio codes previously published in an ERTS bi-monthly report, because the earlier publication did not make use of automatic histogramming for code ranges, and ratio-values were not as accurately calculated.

As an example of the application of ratio codes, consider limestone, represented in the ERSIS library by sample B14004087. The $R_{5,4}$, $R_{6,4}$, $R_{6,5}$, $R_{7,4}$, $R_{7,5}$ and $R_{7,6}$ values calculated from this spectral reflectance curve are, respectively, 1.119, 1.351, 1.207, 1.681, 1.502 and 1.245. The $R_{5.4}$ value of 1.119, represented by the first digit of the ratio code, yields an index number of 4 (see Table 1), which indicates that in the $R_{5,4}$ calculated ratio value, limestone is brighter than only 40% of the other samples in the library data set. An $R_{6,4}$ of 1.351 yields a second digit of 4, etc., resulting in a ratio code for this limestone sample of 446578. The "8" in the sixth digit indicates that limestone is brighter than 80% of the other materials in the library data set in the $R_{7,6}$ ERTS ratio.

If the assumption could be made that the population of the geological data collection is representative of the relative amounts of each target class present in a typical scene, then the phrase "of the other samples in the library data set" could be replaced by "of the materials in the scene." Disallowing this assumption, such a reference number still provides a means for the easy comparison of relative reflectances.

Another reference use of the ratio codes is the prediction of which ratios will best enhance which surface materials. The definition of enhancement in this case is processing by which the target of interest is one of the brightest or darkest objects in the scene. Therefore, those ratios for which a material has a "9" or "0" in the ratio code are most likely to be enhanced. Values of "8" or "1" may also be quite useful, depending on the background materials in the scene. Target materials with all six digits ranging from "2" to "7" are unlikely to be easily discriminated in any single ratio image.

When trying to map a given material, it is useful to know what other materials are likely to produce false recognition. If one knows the ratio ranges for the required material, one can, from Table 2 or any similarly derived table, delineate the index numbers encompassing those values for each ratio. By inspection or by formal computer search, those materials with similar combinations of index numbers can be identified. The results of a demonstration search of the 379 spectra for "look-alikes" of common iron oxides are given in Table 4. Although such a procedure must be viewed in the context of its dependence on laboratory data published in the literature, it is significant that relatively few of the library materials have ratio codes similar to those of iron oxides. It is possible that the soils mistaken for hematite and limonite (see Table 4) do contain those materials, although descriptions of the soils are not complete enough to be certain. Therefore, using spectral ratios calculated from laboratory data, it seems

TABLE 4. RESULTS OF SEARCHES OF LABORATORY SPECTRA FOR MATERIALS WHICH ARE INSEPARABLE FROM SEVERAL IRON OXIDES BY ERTS-MSS RATIO METHODS. Order of code (from left to right is $R_{5,4}$, $R_{6,4}$, $R_{6,5}$, $R_{7,4}$, $R_{7,5}$, $R_{7,6}$)

Subject of Search			Materials With Which Subject Can Be Confused	
Ratio Code Search Range	Name	Ratio Code	Name	Ratio Code
6, 4, 0-2, 3, 1, 1-2	Goethite (74-250 μm, Minn.)	642311	None	——
	(250-1200 μm, Minn.)	640312		
8, 8, 8, 8, 8, 7	Hematite (74-250 μm, Minn.)	888887	Loam, Blakely Clay Type, Dry	888887
7-8, 6-8, 6-9, 5-6, 2-5, 0-2	Limonite (250-1200 μm, Ala.)	889650	Loam, Aiken Clay, Wet	877651
			Loam, Colts Neck Type, Wet	877630
	(74-250 μm, Ala.)	776520	Loam, Greenville Sandy, Dry	876631
	(250-1200 μm, Ala.)	765542	Loam, Santa Barbara Type, Wet	876520
			Loam, Tifton Sandy Type, Wet	876641
			Loam, Hamakua, Heavy Type, Wet	777651
			Loam, Ookola Clay, Wet	776642
			Sand, Colts Neck Loamy, Dry	876641
			Sand, Colts Neck Loamy, Wet	887640
			Yellow Sand, Wet	765542
			Loam, Aiken Clay, Dry	776652
			Loam, Colts Neck Type, Dry	877651
			Loam, Santa Barbara Type, Dry	765642

possible to anticipate other natural targets which may interfere with ratio image or automatic recognition.

3.4 DATA PROCESSING USING SPECTRAL RATIOS

3.4.1 AUTOMATIC RECOGNITION WITH SUPERVISED TRAINING

ERTS digital data was first corrected for additive atmospheric effects (see Section 2.1) and then converted to analog format for use on the Spectral Analysis and Recognition Computer (SPARC). Recognition with supervised training involved the selection of representative target areas in the scene and the training of mean and standard deviation voltages for maximum recognition of each. In this case, the four channels of ERTS data were combined to form six new ratio channels of data, each of which was trained for each target. Due to the variety of dynamic ranges produced by individual ratios, voltage levels are not directly comparable. However, ratio normalization to a well-known target in the scene allows extrapolation to ratio values which are comparable.

Each of eight targets was evaluated in the field to determine vegetation cover and major substrate material. In turn, reflectances of laboratory spectra were combined to correspond appropriately to those targets for which the materials were represented in the ERSIS library. Table 5 shows the target description and ratio ranges from the data with their correlative laboratory spectral ratios. The descriptions of the laboratory spectra indicate the weight that individual spectra were given when combining to approximate the target.

Graphic representation of the absolute value correlations between mean values of data targets and laboratory spectral ratios is given for three cases in Figure 1. "Limestone and grass," as the reference target, has 100% accuracy by definition. It should be noted that the laboratory spectra used were not measured on material actually from the scene, but simply those available in the library. A more critical look at the actual recognition of these target materials in the Wind River Basin will follow in Section 6.

3.4.2 AUTOMATIC RECOGNITION CALIBRATED BY LABORATORY SPECTRA

Ideally, multispectral preprocessing techniques will, in the future, correct for all operational and temporal variations in the data. Temporal ratioing discussed in the following section has shown that extraneous variations can be reduced through appropriate dark object subtraction and ratio normalization even at this early stage. In this respect, accurate determination of atmospheric differences and of the ratio normalization area is extremely important. One approach to the use of laboratory data for identification of surface materials is that of using absolute rather than relative signal values. This method would eliminate the need for supervised training which is susceptible to many errors.

TABLE 5. COMPARISON OF TARGET AND LIBRARY RATIO VALUES FOR AUTOMATIC RECOGNITION OF GEOLOGIC MATERIALS FROM ERTS

	$R_{5,4}$	$R_{6,4}$	$R_{6,5}$	$R_{7,4}$	$R_{7,5}$	$R_{7,6}$
TARGET: Gallatin Limestone exposed on cliff with 50% dry grass cover	1.104-1.336	1.430-1.630	1.123-1.357	1.684-2.316	1.370-1.850	1.213-1.367
LIBRARY: 50% Limestone (B14004087) 50% Dead grass (B01176048)	1.22*	1.53*	1.24*	2.00*	1.61*	1.29*
TARGET: Magnetite and greenstone within Atlantic City Iron Mine	0.900-1.131	0.850-1.037	0.787-1.054	0.401-0.912	0.738-1.039	0.823-1.033
LIBRARY: 50% Magnetite (B09005048) 50% Greenstone (A00261001	0.95	0.91	1.00	0.85	0.93	0.94
TARGET: Precambrian granite of Louis Lake Batholith	1.075-1.267	1.142-1.344	0.986-1.226	0.945-1.578	1.008-1.483	1.072-1.264
LIBRARY: 90% Granite (B09012020 10% Dead grass (B01176048)	1.07	1.14	1.07	1.22	1.12	1.05
TARGET: Triassic Chugwater Formation of redbeds	1.418-1.783	1.847-2.297	1.164-1.400	2.277-2.891	1.406-1.706	1.200-1.354
LIBRARY: 60% Hematite (B09005036) 40% Dead grass (B01176048)	1.57	2.05	1.30	2.55	1.64	1.27
TARGET: Greenstone of the Roundtop Mountain Formation in area not well exposed	1.087-1.240	1.380-1.583	1.126-1.401	0.681-1.271	1.351-1.648	1.168-1.386
LIBRARY: 50% Greenstone (A00261001 50% Dead Grass (B01176048)	1.10	1.32	1.16	1.63	1.39	1.16
TARGET: Permian Phosphoria Formation, NO LIBRARY EQUIVALENT	1.169-1.370	1.433-1.653	1.116-1.312	1.632-2.076	1.330-1.608	1.200-1.341
TARTET: Dense vegetation thought to be chiefly conifers, NO LIBRARY EQUIVALENT	0.910-1.247	1.973-2.356	1.926-2.586	2.960-4.237	2.663-3.730	1.354-1.585
TARGET: Vigorous vegetation in valley of mixed types, NO LIBRARY EQUIVALENT	1.041-1.286	2.417-2.970	1.709-2.284	3.461-4.729	2.686-3.660	1.373-1.553

*Normalization values

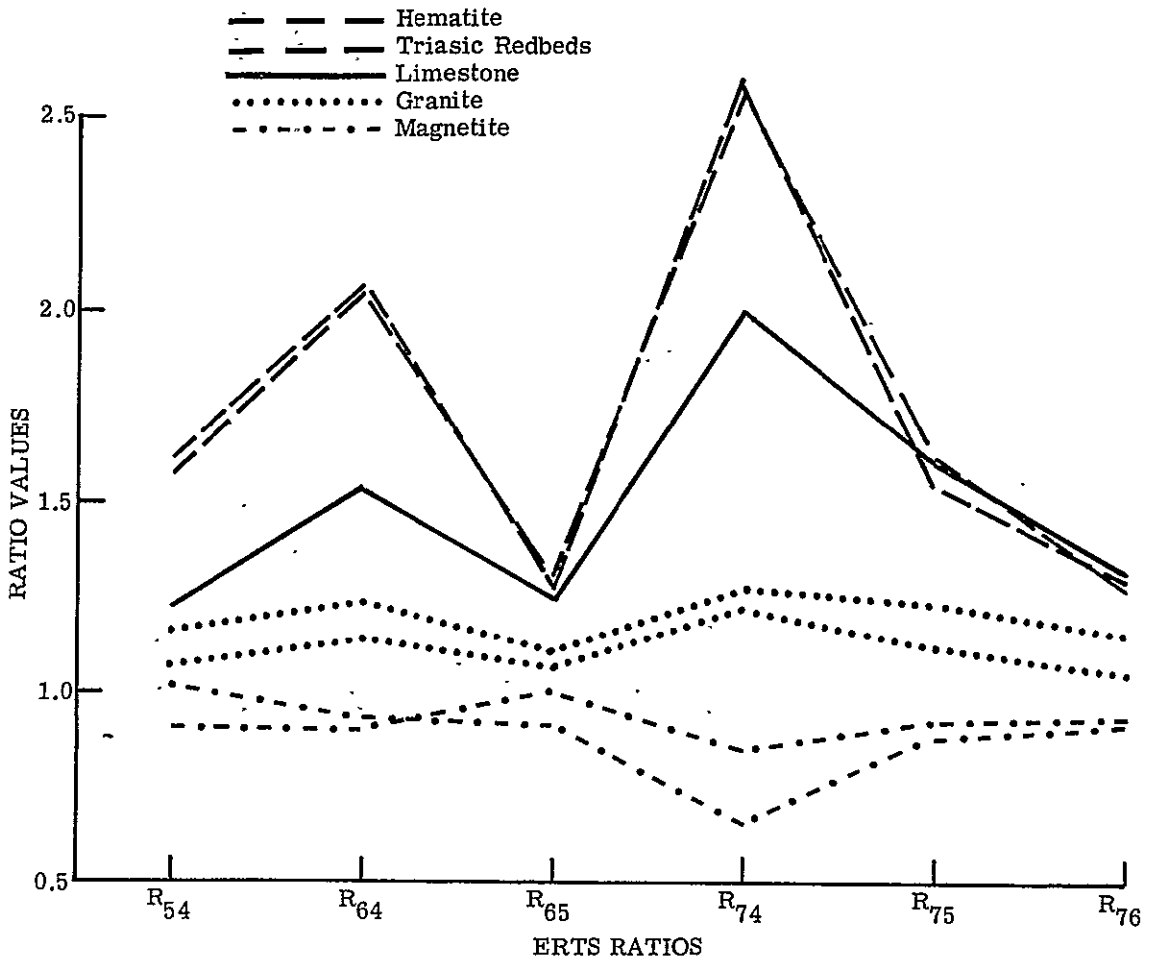

FIGURE 1. COMPARISON OF TARGET MEAN RATIO VALUES WITH REPRESENTATIVE LIBRARY RATIO VALUES. Lines simply connect point values of interest and illustrate trends.

A preliminary attempt at calibrated recognition using laboratory spectra of hematite to recognize the hematite-rich Triassic redbeds was thwarted due to inaccurate ratio normalization. However, extrapolation after improved normalization showed that in this case the recognition which did occur may indeed be accurate.

Normalization was first done on the reference target using ratio values of 100% limestone since aerial photography seemed to show this area to be devoid of vegetation. Ground truth later showed that the area was covered with approximately 50% dead grass. The ratio ranges actually trained are shown in shading in Figure 2. The values for pure hematite, connected by the dashed line, show that only those areas with a minimum of vegetative cover could have been recognized. The sparse recognition within the outcrop area of the Triassic redbeds may very well represent such areas. The results shown in Figure 3 are tabulated for reference in Table 6. Actual recognition produced for Triassic redbeds can be seen inside the geologic boundaries superimposed in Figure 3.

TABLE 6. KEY TO SYMBOLS FOR TEMPORAL RATIO MAPS

Temporal Ratio	Percent Change Between ERTS Passes	Symbol
≤0.80	≤-20%	▩
0.81 to 0.85	-19% to -15%	✖
0.86 to 0.90	-14% to -10%	=
0.91 to 0.95	-9% to -5%	-
0.96 to 1.05	-4% to +5%	Blank
1.06 to 1.10	+6% to +10%	·
1.11 to 1.15	+11% to +15%	*
≥1.16	≥+16%	θ

Two important points to be made in association with this effort are:

(a) Corrected values and mixtures used were determined by ground truth investigation and not by direct fitting of the data.

(b) This correlation is made on an absolute application of automatic procedures, not through artificial selection of dynamic range

This procedure is not mentioned here as a significant result, but as a stimulus to other possible avenues of research.

3.4.3 SINGLE RATIO LEVEL SLICING

There are a finite number of possibilities for using single ratio information for unique discrimination of natural materials. Such a technique is strictly dependent on bandwidth considerations, unique spectra of materials occurring naturally in abundance at the surface, and the applicability of simple mixtures problems. However, for some materials, such as strongly

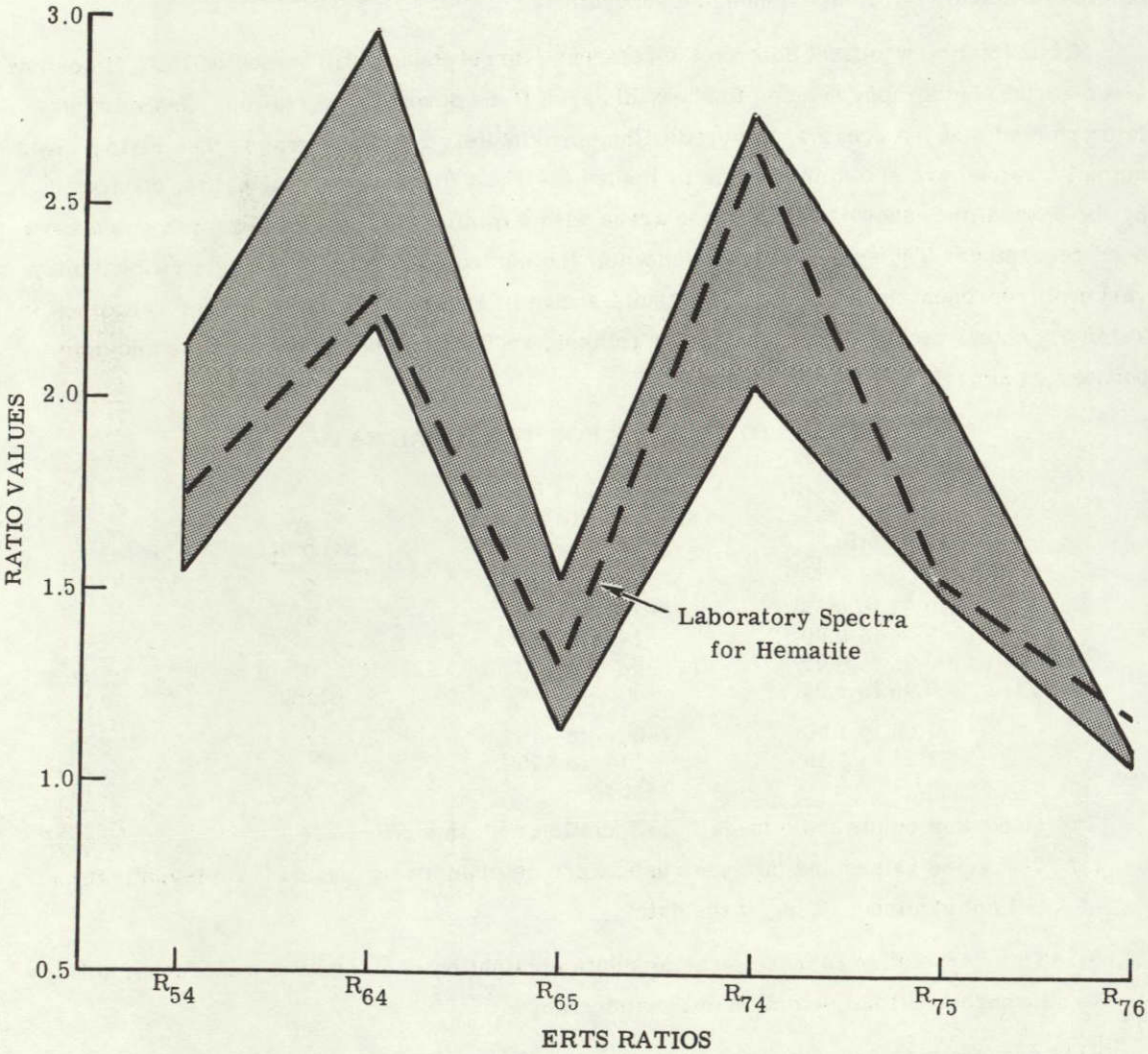

FIGURE 2. RATIO LEVELS COMPARED TO CALCULATED ERTS RATIO FOR 100% HEMATITE CORRESPONDING TO AUTOMATIC RECOGNITION BY CALIBRATION OF TRIASSIC REDBEDS IN FIGURE 3

FIGURE 3. RECOGNITION MAP OF TRIASSIC REDBEDS USING LABORATORY SPECTRA FOR CALIBRATION. (Outline of Triassic formation taken from the U.S.G.S. Geologic Map of Wyoming, 1952.)

pigmented red sediments, a single ratio of even broad bands such as ERTS bands can be used. A practice that would at this time seem promising is multiple ratio recognition with a select number of channels. This procedure is not recommended as an unequivocable tool, but as a viable technique to be applied to emphasize specific spectral responses, particularly to unique responses of alteration products. New earth resource satellites with different bandwidths will allow greater possibilities for finding these successful combinations.

4
AN EXPERIMENTAL CHECK ON ENVIRONMENTAL "NOISE" BY TEMPORAL RATIOING

To evaluate the effectiveness of the ratio method for suppressing atmospheric and solar illumination variations, spectral ratio maps of a subframe area were compared for two ERTS-1 overpasses separated in time by 72 days. The two ERTS frames chosen for this experiment were E-1013-17294 (5 August 1972) and E-1085-17300 (16 October 1972). The area chosen for the temporal ratio map included the iron mine near Atlantic City, Wyoming. Maps of $R_{7,5}$ were produced for both ERTS passes, with dark object subtraction and ratio normalization applied to correct for atmospheric and solar illumination effects. The two spectral ratio maps were merged so that the $R_{7,5}$ map from one ERTS pass was divided by the $R_{7,5}$ map from the other ERTS pass to produce a temporal ratio map. If the empirical atmospheric and solar illumination corrections were perfect, the temporal ratio would be equal to 1.0 for those objects on the ground which did not change between ERTS passes. The 5 August frame had 0% cloud cover and was collected with sun elevation of 54.9° and sun azimuth of 130.2°, whereas the 16 October frame had 20% cloud cover, including some clouds in the subframe area used for the temporal ratio, and was collected with sun elevation of 34.0° and azimuth of 153.4°. The specific test site in the vicinity of the iron mine, which included ten resolution elements used for ratio normalization, was completely cloud free in the 5 August frame, and was approximately 25% covered by cumulus clouds in the 16 October frame.

The path radiance, as indicated from dark object determination, was approximately the same for both frames, although the multiplicative atmospheric and solar illumination variables were significantly different in the two frames. The different atmospheric states (as evidenced by cloud cover) and sun position represented in the two data sets offered a fairly rigorous test of the empirical correction steps in the ratio method.

The procedure for testing the atmospheric and solar illumination invariance of the ratio method began with an estimate of the number of spatial resolution elements (each approximately 100 meters in diameter) within the scene which: (a) had greater than 50% vegetative cover in the 5 August frame, and (b) were covered by clouds in either frame. The vegetation in the

Atlantic City area is primarily a mixture of coniferous and deciduous trees, coarse grass and sage. Sparsely vegetated areas were delineated by thresholding the 5 August $R_{7,5}$ ratio map to include only those spectral resolution elements with values below 1.20. This procedure appeared to approximately delineate areas of less than 50% vegetation cover, as verified by ground photographs and observations made during the 21-27 July 1973 field trip. Cloud areas were delineated easily by ratioing ERTS-MSS Channel 7 for the 16 October frame to the same channel for the 5 August frame.

Elements remaining after elimination of vegetated areas and cloud-covered areas are called ground invariant (GI) elements. These represent the portion of the test area which is suspected to have changed less than ±5% in spectral radiance between the two ERTS passes and are shown in the map in Figure 4. Out of a total of 25,125 points in the entire scene, 11,032 points were considered to be GI elements.

All of the temporal ratio maps used here were formed with the 16 October data in the numerator and the 5 August data in the denominator. The procedure was used to produce temporal ratios of single channel data uncorrected for atmospheric and illumination effects and of ratioed data before and after dark object subtraction and ratio normalization. Figures 5a and 5b show single channel temporal ratios for ERTS-MSS Channel 7 and Channel 5, respectively. In this and all subsequent temporal ratio maps, light tones represent small changes (smaller departures from the value 1.0) and dark tones represent large changes; a key to specific symbols is included in Table 6.

In the Channel 7 temporal ratio (see Figure 5a), only 361 elements in the scene, or 3.27% of the ground invariant elements, changed between ERTS passes by ±5% or less (corresponding to a temporal ratio between 0.96 and 1.05). In the channel 5 temporal ratio map shown in Figure 5b, there were 1,122 such elements, or 10.17% of the GI elements. Considering that path radiance was found to be approximately the same for both passes, the greater change in Channel 7 leads to the conclusion that the change in solar illumination was greater than the change in atmospheric parameters between 5 August and 16 October for this test site.

Figure 6a shows a temporal ratio map of an $R_{7,5}$ spectral ratio uncorrected by dark object subtraction and ratio normalization. The number of elements which changed by ±5% or less between ERTS passes in this case was 2,320, or 21.02% of the GI elements. Thus, even an uncorrected $R_{7,5}$ spectral ratio map was more independent of atmospheric and solar illumination than single channel radiance maps. Shown inFigure 6b is a temporal ratio map of an $R_{7,5}$ spectral ratio corrected by both dark object subtraction and ratio normalization. For this case, the number of elements which changed by ±5% or less between ERTS passes was 11,032 (37.30% of the GI elements). Therefore, the corrective steps of the ratio method produced a map which was more independent of atmospheric and solar illumination than either the uncorrected spectral ratio map or the maps of single channel radiances.

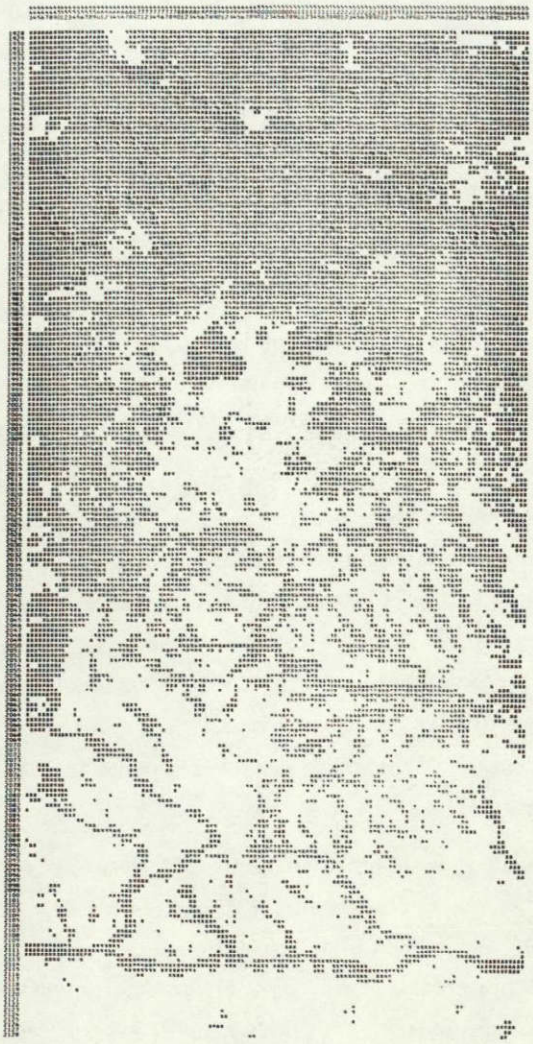

FIGURE 4. MAP OF ESTIMATED GROUND INVARIANT ELEMENTS BETWEEN 5 AUGUST AND 16 OCTOBER 1972 ERTS PASSES OVER TEST SITE NEAR ATLANTIC CITY, WYOMING. Dark symbols represent elements in the scene which have >50% vegetation cover, or which are cloud-covered in the 16 October 1972 ERTS frame. Blank represents elements in the scene which are suspected to have changed less than 5% in spectral reflectance between ERTS passes; these are the estimated ground invariant (GI) elements.

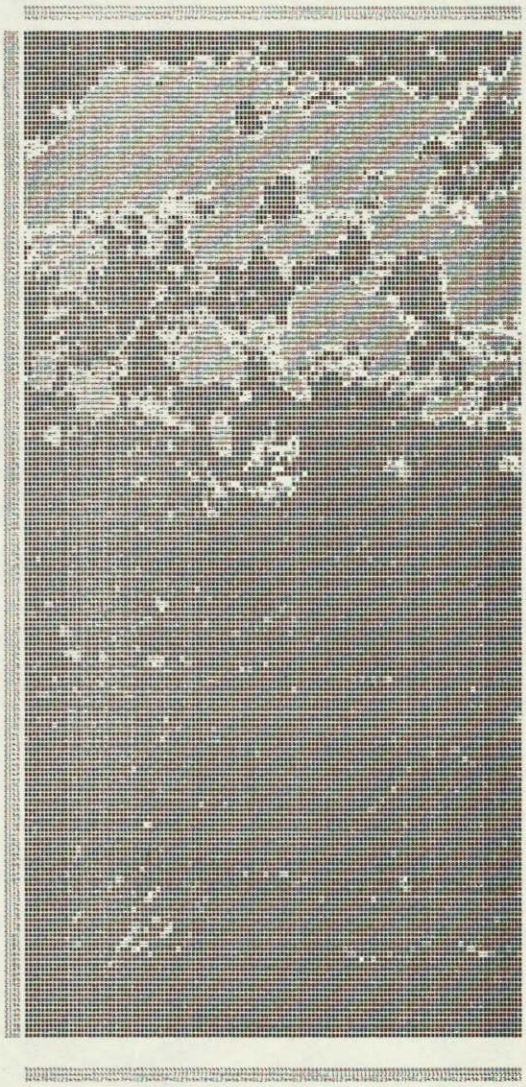

FIGURE 5a.

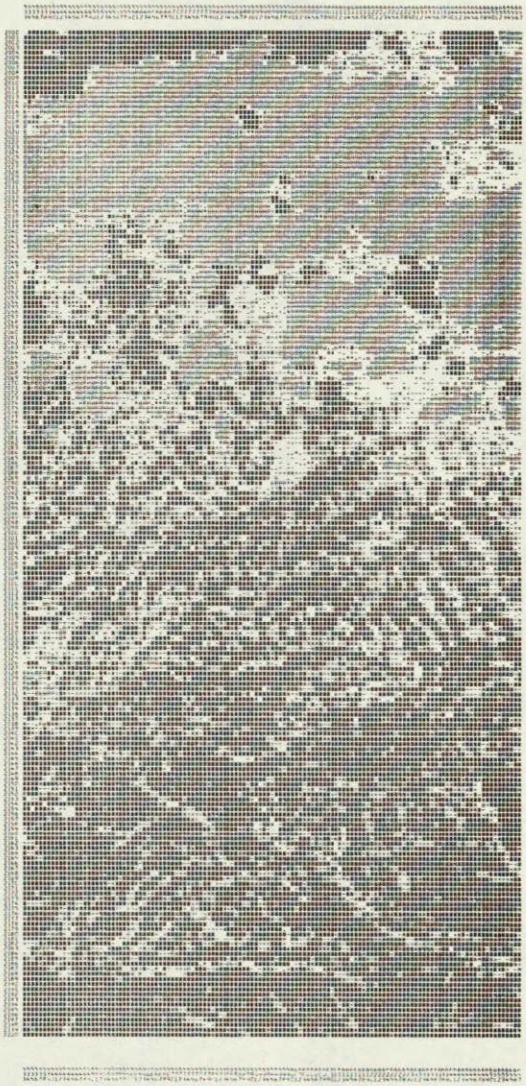

FIGURE 5b.

FIGURE 5. TEMPORAL RATIO MAPS OF ERTS MSS CHANNELS 7(5a) AND 5(5b) (16 OCTOBER 1972 FRAME DIVIDED BY 5 AUGUST 1972 FRAME) FOR TEST SITE NEAR ATLANTIC CITY, WYOMING. Lighter-toned symbols represent less change in the scene between ERTS passes (see Table 6 for key).

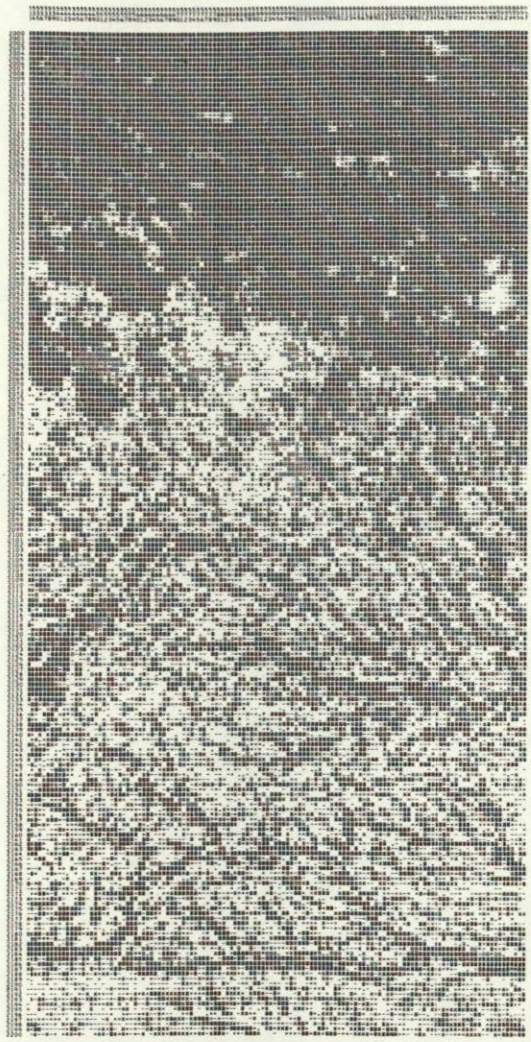

FIGURE 6a

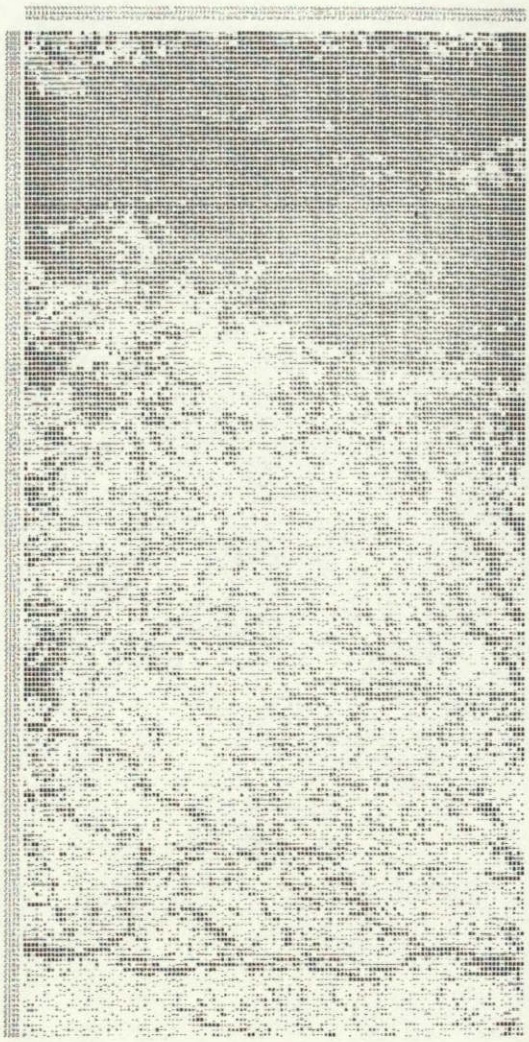

FIGURE 6b

FIGURE 6. TEMPORAL RATIO MAPS OF UNCORRECTED R_{75}(6a) AND CORRECTED (6b) SPECTRAL RATIOS (16 OCTOBER 1972 FRAME DIVIDED BY 5 AUGUST 1972 FRAME) FOR TEST SITE NEAR ATLANTIC CITY, WYOMING. Lighter-toned symbols represent less change in the scene between ERTS passes (see Table 6 for key).

The temporal ratio procedure as used here is only an approximate answer to absolute correction for atmospheric and solar illumination variability. Table 7 shows the number of points on the ground which changed ±5% or less, ±10%, or less, and ±15% or less between ERTS passes, expressed as a percentage of GI elements. This shows that the corrected $R_{7,5}$ spectral ratio for this test site was invariant for 5 August and 16 October ERTS passes to within ±10% for 70% of the GI elements, and to within ±15% for practically all of the GI elements (97%).

TABLE 7. ESTIMATE OF R_{75} SPECTRAL RATIO ABSOLUTE INVARIANCE CORRECTED BY DARK OBJECT SUBTRACTION AND RATIO NORMALIZATION. Temporal ratio map of 16 October 72 and 5 August 72 ERTS passes over a test site near Atlantic City, Wyoming.

Changes in Corrected R_{75} Between ERTS Passes (%)	Number of Elements Undergoing Change	Estimated Ground Invariant Elements* (%)
±5	4,115	37.30
±10	7,745	70.20
±15	10,682	96.83

*11,032 element total.

Sources of possible error for these estimates are:

(a) Some of the estimated GI elements could have changed more than ±5% during the ERTS passes through natural or unnatural causes.

(b) The merging process is estimated to be accurate to within about two spatial resolution elements, which means that some points expected to be GI elements may show change only because of errors in registration between pixels from the two data sets.

(c) No attempt was made to discount points with small change that occurred in non-GI elements, though a comparison of Figures 4 and 6 shows that the vast majority of elements exhibiting small change in corrected $R_{7,5}$ values are GI elements

The first two sources of error make the results of Figure 5, Figure 6, and Table 7 appear worse than they actually may be, whereas the third error source makes them appear better than the actual result. Overall, it is suspected that the first two sources of error dominated, yielding worse errors than actually occurred. These considerations and the above quantitative results indicate that the corrected $R_{7,5}$ ratio map was independent of atmospheric and illumination effects to within ±10% or better for this experiment.

It is beyond the scope of this contract to perform more rigorous tests of the ability of the spectral ratio methods to suppress environmental "noise." Further research is recommended. It should be noted that the dark object and ratio normalization procedure designed primarily to suppress environmental "noise" will also suppress both additive and multiplicative electronic

offset and gain variations between sets of data gathered at different times and places. For these reasons, it is recommended that for geological remote sensing in the 0.4-2.5 μm region, at least dark object subtraction (for satellite and high altitude aircraft data) and ratio normalization be employed if either absolute ratio values or extension or recognition results over data sets separated in space and time are called for.

If the corrected spectral ratio maps resulting from Eq. (5) are independent of environmental and system "noise" to better than 10%, the temporal ratioing method described above may become an important tool for remote-sensing problems requiring quantitative change detection. The immediate application suggested by this experiment is the monitoring of open pit mining. Other problems related to pollution monitoring may also be aided by the temporal ratio method, especially for pollution law enforcement in courts of law, for which the separation of "noise" from on-the-ground changes must be accomplished beyond a reasonable doubt.

GEOLOGIC BACKGROUND

5.1 THE IMPORTANCE OF SURFACE EXPOSURES OF IRON OXIDES

The most well demonstrated geologic use of spectral ratioing thus far is the mapping of the red and yellow colors indicative of hematite, goethite, and limonite, using an ERTS $R_{5,4}$ ratio image. Table 4 indicates that these ferric-oxide minerals can theoretically be discriminated from each other using additional ERTS ratios. Future laboratory and scanner data may be able to provide this capability.

Locke [8] was one of the first to notice correlations of secondary iron-oxide colors to the sulfides from which the iron residual deposits were derived. Weiser [9] showed that colors of synthetic hydrous ferric oxides reflect the chemical conditions under which colloidal iron particles were initially precipitated. Copper and iron ore bodies were the first to receive much attention with regard to surface iron oxide exposures. Blanchard [10] has perhaps given the best guidelines for the use of iron-oxide mapping related to copper and iron prospecting. He carefully limited its usefulness with the following conclusions:

1. Although reddish iron-oxide colors most commonly point to hematite, and orange-yellow-buff-ochreous colors to geothite and jarosite, no iron-oxide color is a completely dependable representative of a specific ferric oxide hydrate or supergene mineral.
2. Although a particular iron-oxide color may be characteristic of a specific sulfide in a given district, the same color may not represent the same parentage throughout that district.

3. Several iron oxides of contrasting colors may be associated with a single deposit.
4. Even when color is useful in determining the iron-oxide parentage, it remains subordinate to other physical characteristics useful for this purpose.

The use of outcrop iron-oxide colors as guides to lead and zinc ore has been investigated by Kelly [11]. In some of the areas Kelly visited, he found that the colors of iron precipitates in the outcrops bore a definite relation to original lead, zinc, and iron sulfides. Referring to their Munsell designations, Kelly found dusky reds (5R 3/4 to 10R 2/2) associated with galena; light browns (5YR 5/6) to yellowish oranges (10YR 3/4) with sphalerite; and dusky browns (5YR 4/4) to reddish browns (10R 3/4) with pyrite, except when oxidized in a reactive gangue, in which case yellowish-orange (10YR 6/6) limonite can also occur. He also found that a color indicative of ore in one area may be insignificant or entirely absent in another. Kelly concludes that the iron-oxide colors may be locally quite useful in certain districts, but should not be used indiscriminantly without allowance for local variations.

Gold is also sometimes associated with surface iron oxides. Rowan et al. [12] have used a color composite of three ERTS ratio images to map hydrothermally altered areas in South-Central Nevada over a known gold deposit. The limonitic soil directly above the deposit has a unique color in the color ratio composite, but could not be discriminated from other areas in the scene by examining photos or single channel images. The largest mined deposit of "invisible" gold, the Carlin gold deposit in Western Nevada, is disseminated in a yellowish limonitic soil that should be similarly enhancible by ERTS ratio images.

Uranium is another metal which often displays an association between ore deposit and surface iron oxides. Shockey [13] used the term geochemical cell to describe the invasion of reduced, carbonaceous, and pyritiferous sandstone and uranium ore bodies by oxygenated ground water. A well developed geochemical cell is shaped like a tongue, pointed down the hydrostatic gradient. The geochemical cell itself often has colorful iron oxides in the interior which can be exposed at the surface. The cell size is usually very large in comparison to the size of the mineralized "fronts," which occur along the edges of the cell and along irregularities on the upper and lower surface [14]. Primary uranium minerals, when oxidized to the hexavalent uranyl ion by oxygenated water, are mobile in weakly acidic solutions or in neutral or alkaline solutions if carbonate ions are present [15]. The uranium can be reduced by a number of chemical agents, including pyrite and organic matter, and deposited as uraninite or a hydrate.

There may even be a role for iron-oxide mapping in exploration for petroleum and natural gas. A recent paper by Donovan [16] on the Cement, Oklahoma oil field has proven that pronounced bleaching of red beds at the surface can be caused by petroleum microseepage along structural zones of weakness. The typical Rush Springs sandstone is red-brown (10R 4/6),

but has been altered to pink (5YR 8/1 to 5YR 7/2), yellow (5Y 7/2 to 5Y 8/4) and almost white (5Y 8/1 to N8). He explains that hydrogen sulfide was probably liberated by the alteration of sulfate to carbonates by microscopic seepate of hydrocarbons along faults through a gypsum-rich stratum. It then acted as the reducing agent which bleached the surface red beds. If the reverse effect could occur, i.e., reduction of subsurface red beds by hydrocarbon seepage and reoxidation of the vertically transported products, iron oxides could form at the surface.

Though these applications of iron oxide mapping require similar spectral bands in multispectral scanners, they differ greatly in spatial resolution requirements. The strongly oxidized surface alterations of copper, iron, lead and zinc deposits, which typically cover areas from a few to a few hundred meters in diameter, would suggest the need for scanners with an instantaneous field of view on the order of five or ten meters. Aircraft scanners can accomplish this resolution and better. Satellite scanner resolution may be limited by restrictions on the possible size of the instantaneous field of view. Although regions of strong alteration are typically small, the outcrop or soil surrounding and affected by them may be observable with enhancement techniques, thus raising the possibility that improved spectral techniques may reduce the restrictive spatial requirements for these ore bodies.

The gold, uranium, and petroleum occurrences cited are different, in that alteration patterns can be a hundred meters to several kilometers in areal extent. For these applications, ERTS and SKYLAB resolution seem particularly well suited. The approximately 80-meter spatial resolution of ERTS permits the coverage of vast areas in a single frame of data and also tends to "filter out" some of the smaller surface exposures of iron oxides that would seem to have lower probabilities of leading to large ore deposits.

5.2 SELECTION AND DESCRIPTION OF TEST SITE

The Wind River Basin and the encompassing mountain ranges in central Wyoming have a semi-arid climate and are, in general, sparsely vegetated. This area was chosen as a demonstration site for a combination of geologic and geographic characteristics amenable to the task of discriminating iron compounds. The geographical location of the Wind River Basin provides, along with appropriate climate, an area of relatively high elevation, allowing fewer atmospheric problems for an experimental study of this type. The area contains a variety of rock types, as well as known concentrations of iron-oxide rich exposures. Precambrian igneous and metamorphic rocks available near the Atlantic City Iron Mine, include mafic dikes, magnetite, greenstone, meta-andesite, and serpentinite. Among the Mesozoic formations present in the Triassic Chugwater group, containing hematite-rich sands, siltstones and shales which are ostentatiously exposed as tilted red layers at the rims of the basin. A third major occurrence of iron oxide is in the limonitic soils and altered Tertiary arkose associated with secondary uranium deposits

of the Gas Hills area in the eastern Wind River basin. The possibility of recognizing these and the hope of finding new occurrences of important minerals made this area ideal for a remote-sensing investigation.

Geologic Description

The Wind River Basin is both a topographic low and a structural basin, surrounded by mountains with Precambrian granite cores. (Figure 7) Tertiary sediments make up most of the interior exposure, with Quaternary sediments found locally within the basin and along drainage courses. Paleozoic and Mesozoic sediments are exposed at the perimeter of the basin and in local structural highs. The Absaroka Mountains to the northwest of the basin are composed of layered Tertiary volcanics which contributed significant amounts of volcanic debris to the Tertiary sediments of the region. The Beaver Escarpment of Lower Tertiary sediments borders the basin to the southeast and is breached by the isolated knobs of the Precambrian Granite Mountains. Winding its way southeast and then turning north, the Wind River empties into the Boysen Reservoir, which in turn empties into the Big Horn River. Many of the tributaries running into the Wind River from the east are dry ribbons of sand for much of the year, including the time that the data were collected in August.

The area is already well known for its oil, gas, and uranium deposits in the basin proper. The Atlantic City Iron Mine in the Precambrian metamorphics to the south is also of great economic importance, as were the gold deposits in nearby South Pass City. The stratigraphic sequence of the Wind River Basin starts with the Precambrian granite cores of the surrounding mountain ranges and the associated metamorphics and iron formation. Above these, lying unconformably on the metamorphics and granites, is the basal Flathead quartzite, a red to gray sandstone which is sometimes conglomeritic and cemented with iron oxide. The greenish gray calcareous shales of the Gros Ventre formation are transitional between the Flathead and the Gallatin Formation, an Upper Cambrian carbonate which is well known for its Open Door Limestone interformational conglomerate. Above the Gallatin, the Bighorn dolomite and Madison limestone, Upper Ordovician and Lower Mississippian respectively, are exposed along the flanks of the Wind River range, Owl Creek range, and Big Horn mountains. These three formations, in their combined thickness, make up an extensive exposure of carbonates, although much of their area is covered with dense vegetation. Separating the Madison limestone from the massive Pennsylvanian sandstone above is a thin deposit of red shales and silts, the Amsden Formation. The overlying Tensleep Sandstone is buff-colored, and often cemented with carbonate. Above this the Phosphoria Formation is a conglomeration of cherty dolomites, limestones, and phosphatic shales and siltstones, and marks the end of Paleozoic rock-stratigraphic units.

Although the Dinwoody Formation of Early Triassic time is sometimes differentiated from the overlying Red Peak member of the Chugwater Formation by a transition upwards from green

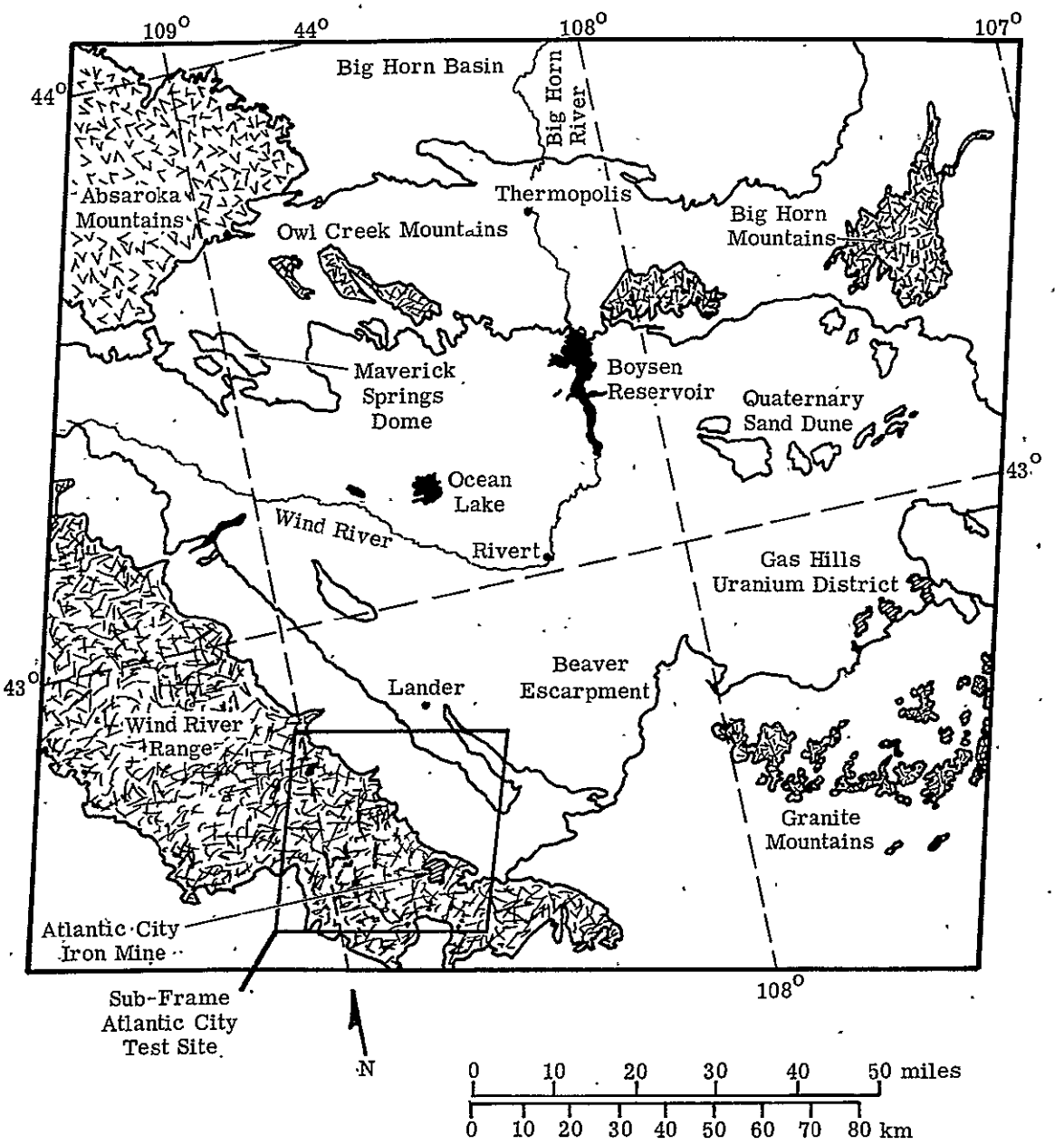

FIGURE 7. WIND RIVER BASIN, WYOMING-AREA OF ERTS COVERAGE IN FRAME E-1013-17294 WITH ATLANTIC CITY TEST SITE ANNOTATED

to red, this is not necessarily a precise delineation. Workers such as Love [17] have reported the reduction of iron in some parts of the Red Peak member causing alteration from red to green in parts of this formation also. X-ray studies by Picard [18] have documented more important mineralogical differences, such as an abrupt increase in quartz and increased feldspar, calcite and other minerals.

Mineralogy and grain size considerations are of great importance in dealing with members of the Triassic Chugwater formation for this report. The correct interpretation of recognition due to intense color and that due to increased iron concentration is important in the field statement of the conclusions for mapping iron compounds. It has been reported by Picard [19] that in both red and drab (green) rocks the percentage of total iron increases with decreasing grain size. Iron in the Chugwater Formation occurs in many different associations, several of which add to the red color. Hematite, the dominant iron-oxide mineral, occurs as individual grains, as "pigment" in matrix material, and as grain coatings on the larger sand fraction [19]. Within the Chugwater Formation, shale, silt, and sandy members are present, allowing a range of grain sizes and variable iron content. Although red coloring in clastic sediments is often thought of as being associated with iron content, its intensity does not necessarily correlate with the relative percentage of Fe^{3+}. The Alcova limestone member, a thin persistent layer of limestone, caps the formation and helps hold up the red cuestas in evidence at many exposures of this formation.

The Nugget Sandstone, a salmon to deep-orange colored sandstone above the Chugwater, has a very small percentage of total iron, having very little clay-size material, but the hematite coating of these sands highly influences their perceptive color. The Gypsum Springs Formation, a red shale and siltstone with associated massive gypsum and dolomite, overlies the Nugget as a narrow division between it and the Lower Sundance. In the southern portion of the Wind River Basin the Lower Sundance is a fine-grained pink to gray sandstone. In the northern exposures and in the Upper Sundance member in the south, the formation is characteristically gray to pale green with interbedded shales and narrow limestone beds.

These and younger Mesozoic deposits are chiefly clastic sediments, reflecting the active tectonism and ample source material of this time. Deposition of the Morrison Formation in the late Jurassic period continued into the early Cretaceous with the deposition of the Cloverly Formation. In general, both these formations are interbedded sandstones and brightly-colored variegated shale and claystone, with little evidence for distinction between them [20]. The overlying dark organic shale, also deposited during the early Cretaceous, is known as the Thermopolis Shale. Lower Cretaceous sediments thin northwestward within the Wind River Basin, and therefore formations exposed in the Owl Creek uplift differ in lithology from those along the Wind River Range.

The Mowry Formation, predominantly black shale but also containing sands and abundant bentonite layers, weathers to a silver-gray and often supports conifer trees on its outcrops [21]. Above the Mowry, the Frontier Formation is a great thickness of Upper Cretaceous salt-and-pepper sandstone with interlayered black shales. The contact between the Frontier and the overlying Cody Formation is marked by a lenticular, yet persistent and distinctive, sandstone marker. The lower half of the Cody is predominantly shale and the upper half interbedded shales and sands. The shales of the Cody are usually exposed in broad, flat valleys and, as in the Mowry, weather to light gray. The sands of the Cody weather to light-buff and develop slightly more topographic relief [22].

The Mesaverde Formation, the Lance Formation and the stratigraphic interval in between referred to as the Lewis-Meeteetse, are a wide variety of alternating clastics. In the Mesaverde, individual beds are lenticular and can be traced laterally only for short distances [22].

In some areas the Lance and Meeteetse are not even differentiated in geologic mapping, and the nonpersistent thicknesses of lithologic units with this Upper Cretaceous group make it an unlikely target for remote sensing considerations [22].

In late Cretaceous time, the Laramide orogeny caused downwarping of the basin itself with doming of parts of the surrounding areas. Finally, in early Eocene the uplifting of high mountain regions around the basin caused the shedding of great thicknesses of fluviatile and lacustrine sediments into the subsiding basin [20]. Tertiary volcanics contributed greatly to the accumulation of sediments during that time, with centers of volcanic activity both in the Absarokas and the Rattle Snake Hills. These Tertiary sediments, as they are presently distributed, are of great importance to geologic investigations by remote sensing, for they immediately underlay the major portion of the Wind River Basin.

A study of the heavy-mineral associations within the Paleocene and Eocene rocks of the Wind River Basin [23] has been used in documenting the influence of volcanic assemblages and the subsequent exposure of the surrounding Precambrian cores, insofar as they shed characteristic heavy minerals into the lacustrine sediments deposited in the basin. Initially, Paleozoic and Mesozoic sediments were the source of Tertiary deposits in the basin. The Fort Union Formation, deposited in Paleocene time, was made up chiefly of reworked sediments, resulting in a light-gray to yellowish-gray and tan mudstone and sandstone, locally cemented with limonite, and including pebble and cobble conglomerates. It is the presence of these conglomerates which sets this formation apart from Upper Cretaceous sediments and is given as evidence for renewed tectonism at this time [24].

The Fort Union Formation outcrops within the Wind River Basin in basin-margin folds and in some exposures of undulations in the basin proper. The formation is bounded by angular

discordance with Upper Cretaceous and Lower Eocene formations. The extensive thickness and associated limonite cement and ferruginous concretions [21] make exposures of the Fort Union of particular interest in the effort to test our ability to remotely sense iron compounds. The outcrop of this formation at Castle Gardens is known to be highly-stained (10YR 6/6) and well exposed.

The Wind River Formation and its stratigraphic equivalents are usually assigned to the Lower Eocene, and are reportedly derived less from Paleozoic and Mesozoic marine sediments than from metamorphic and igneous rocks which were in turn exposed by continued uplift and degradation [23]. The Wind River coarse clastics, called "first-cycle medium- to coarse-grained arkosic debris" by Denson and Pipiringos [23], consist of poorly-sorted yellowish-orange feldspar-rich sandstone commonly containing calcareous or limonitic cement, pebble conglomerates and red-banded mudstone, and appear to have had their major source at the southern margin of the Wind River Basin [24]. On the basis of heavy mineral analysis, Denson and Pipiringos [23] would generalize that Paleocene and Lower Eocene sediments, including the lower Wind River Formation, were largely the products of the weathering of the surrounding highlands and reflected tectonism and uplift. Non-opaque heavy minerals such as blue-green hornblende, epidote and garnet are the assemblage indicating a provence of Plutonic rocks. Volcanics coming from the vicinity of the Absaroka Mountains contributed green-brown hornblende and augite to upper Eocene Age rocks, particularly in the northwestern part of the basin. Euhedral, transparent zircons in Upper Eocene sediments, are attributed to volcanics contributed by the Rattlesnake Hills volcanic region [23].

The occurrence of heavy minerals in these deposits is of interest in the context of the availability of iron-rich minerals for later oxidation or alteration. The Upper and Middle-Upper Eocene rocks described by Van Houten [24] are also well exposed in several areas, particularly along the front of the Beaver Escarpment. These are pale greenish-yellow, pale olive, and yellowish-gray volcanic-rich rocks containing some bentonite with an accumulation of as much as 700 feet, although local thickness depends on the relief of the erosional unconformity below the overlying Oligocene White River formation [24].

During the Oligocene Age aggradation occurred within the basin, with the accumulation of volcanic-rich arkosic sand in the valleys developed during the prior period of erosion. Even those sediments deposited in the southeastern section of the basin contain great accumulations of materials originating in the Yellowstone-Absaroka area. Much of the White River Formation, a yellowish-gray to grayish-orange tuffaceous and bentonitic mudstone with fine-grained sandstones and arkosic sandstone, was deposited by streams and mudflows transporting andesitic volcanic debris [24]. Some of the uranium concentrated in arkosic sandstones in the underlying Wind River Formation is thought to have been leached from these volcanic debris deposits [17].

Miocene rocks reported to underlay the Sweetwater plateau have been described as "massive, light gray to yellowish-gray and grayish-orange well sorted volcanic-rich medium- to fine-grained sandstone with well rounded grains . . . . Locally the sandstone contains considerable calcareous cement, . . ." [24]. These and some Pliocene deposits are found only on the Sweetwater Plateau to the southeast of the Wind River Basin.

Quarternary deposits, including lag gravels, valley fill, sand dunes and some red valley fill directly derived from Triassic sediments, show close association with present drainage patterns and topography. Much of that area used for agriculture and watered by present day drainage systems is mapped as Quaternary alluvium. In many areas of the basin, particularly in the northeast section, mesas are capped with Quaternary gravels where Tertiary formations are actually exposed directly below. These gravels are very varied in color and petrology.

The abundant clastics of the Wind River Basin, many of them geologically young and derived from primary and secondary sources with ample iron-rich minerals, provide many opportunities for recognizing the influence of iron-oxide concentration on surface exposures. Precambrian metamorphics, granites, and Tertiary volcanics are all primary sources for heavy minerals, while the reworking of iron-rich sediments is well exemplified by the red Quaternary alluvium deposited directly downslope from Triassic redbed deposits. Concentrations, remobilization and oxidation of the material provided by these sources may all be important to the development of economic deposits which could be of importance within the basin. Specifically, hydrothermal alteration, epigenetic oxidation and the remobilization of iron accompanying reduction by hydrocarbon seepage can all be indicators of possible mineral or energy resources.

6
RESULTS OF MULTISPECTRAL STUDIES IN THE WIND RIVER BASIN, WYOMING

6.1 SINGLE RATIO CONTRAST ENHANCEMENT AND DENSITY SLICING

Figure 8 is an analog image produced on the SPARC of a ratio ERTS Channel 5/Channel 4 [25]. The ability to recognize the Triassic redbeds uniquely in this single ratio is based on hematite's increasing reflectance with increasing wavelength in the 0.5-0.7 μm range. The tone of the material in this ratio image was predicted from data bank values, which indicated that in the $R_{5,4}$ ratio image hematite would be brighter than 80% of the materials represented in the data bank. The brightest areas within the redbed exposure correlate to cliff rims and other areas of little vegetative cover. A density slice showing the isolation and mapping of the

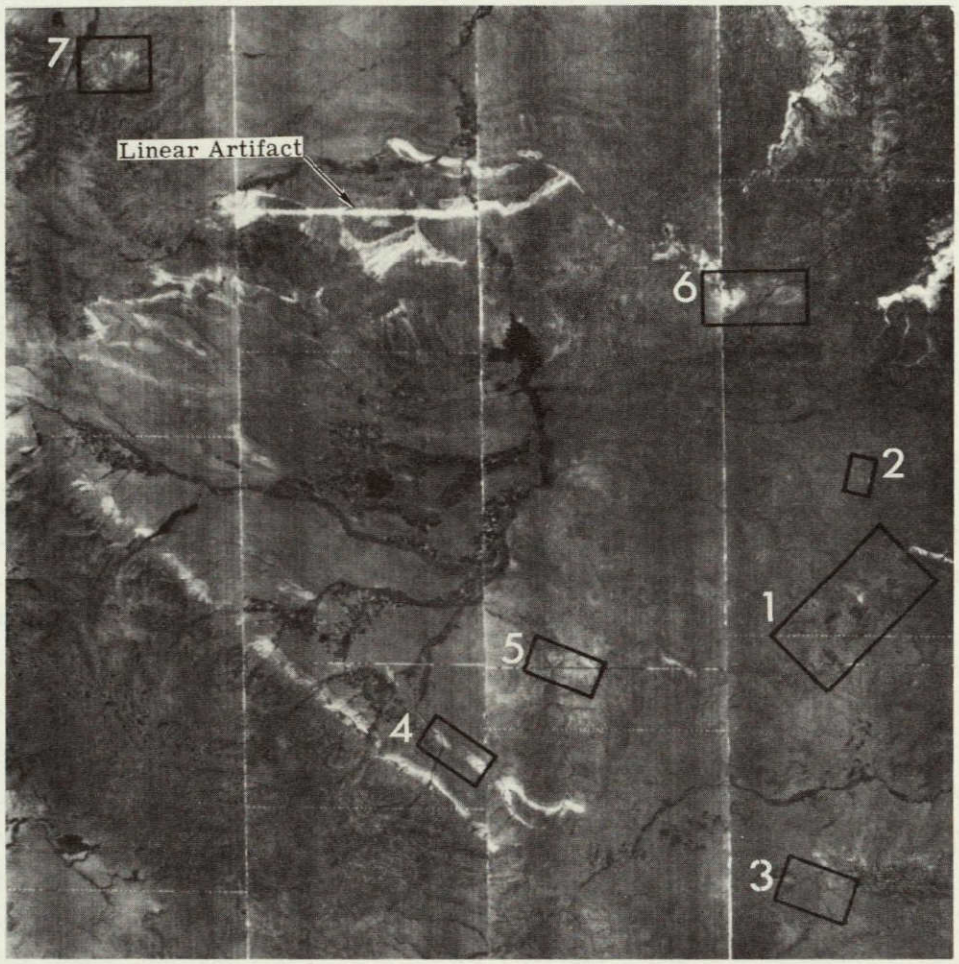

FIGURE 8. ERTS MSS CHAN 5/CHAN 4 ANALOG RATIO IMAGE OF THE WIND RIVER BASIN, WYOMING

voltage level representing this ratio can be seen in Figure 9, demonstrating the accuracy with which this stratigraphic unit was uniquely recognized. (Compare this figure with the outline from the geologic map shown in Figure 14.) A continuous tone image of the ratio not only shows this formation well, but indicates there may be other areas of interest due to their higher than average values. Successively lower voltage density slices should recognize smaller, yet significant, levels of iron-oxide influence at the surface, to the extent that it appreciably influences the color.

Features labeled in Figure 8 show some areas of interest in the Wind River Basin ERTS $R_{5,4}$ ratio images. Feature 1 is the Gas Hills uranium district, in the southeastern part of the Wind River Basin. Open pit uranium mines are dark, probably because of the grayish arkosic sediments exposed in the pit bottoms. The altered Puddle Springs Arkose (Eocene), yellowish-gray to greenish-gray in color, shows as slightly lighter-toned on the ratio image than the older Pre-Wind River sediments. The bright area is a small exposure of Triassic redbed. Feature 2, light-toned in Figure 8, occurs where altered alluvial sands are present, and is the site of a small uranium mine (Twin Arrow). Feature 3 is the Crook's Gap area. Some of the slightly lighter-toned areas may be related to known uranium prospects. These three features indicate that, relative to primary redbeds, alteration products associated with uranium deposits are subtle features in an ERTS $R_{5,4}$ ratio image.

Feature 4 shows part of the Sage Creek Anticline, where Triassic redbeds have been exposed at the surface. Oil fields (Dallas field in the northwestern part of this feature) are located in the bright areas because of the coincidence in this case of structural traps and exposed redbeds resulting from the anticline. Feature 5 is the Beaver Creek Dome (Beaver Creek oil field is on the northwestern extremity of this dome), which has Tertiary Age redbeds exposed at the surface. Feature 6 is an east-trending elliptical feature, bounded on the north by a major fault. The major axis of this ellipse coincides with the axis of a syncline. The ellipse is caused by yellow, orange, and reddish iron oxides in Tertiary sediments. The iron oxides appear locally to be strata bound. Sulphur springs are located in the western part of this feature, and a new gas well (in the Cody shale) has recently been drilled in the eastern part, at Lost Cabin. Features 4, 5 and 6 offer encouragement that mapping pattersn of surface iron oxides may yield information that will be helpful in oil and gas explorations.

Finally, Feature 7 shows light tones surrounding Soapy Dale Peak, in the Absaroka Mountains, with a light-toned central peak. The authors have not visited this area, but we think that the iron oxides indicated in this $R_{5,4}$ ratio image are related to the volcanic rocks known to occur in this region. The iron oxides may simply represent weathering products of intermediate to basic volcanic flows. However, since this area is twenty miles east of Kirwin district

FIGURE 9. DENSITY SLICE OF ERTS MSS CHAN 5/CHAN 4 OF THE WIND RIVER BASIN, WYOMING

(just off this image), where molydenum and copper deposits are being mined, these iron oxides could be indicative of another porphyry deposit. Nevertheless, feature 7 is the type of anomaly that alteration in igneous terrain is expected to produce in $R_{5,4}$ ratio images.

Geologists are not accustomed to interpreting the large-scale surface patterns of iron oxides, and much remains to be learned before the implications of these data can be fully assessed. Though mineral exploration will probably be the first geologic discipline to benefit from this tool, other applications should follow. For example, mapping the lateral extent of oxidized beds from intermittent stream sediments deposited during savannah climates of the past should be helpful in hydrology.

6.2 AUTOMATIC RECOGNITION BASED ON SUPERVISED TRAINING

The success of any automatic recognition technique is dependent on the natural variations within a material, its distribution and its exposure. Clearly vegetation cover can alter the sensed reflectance of a well-distributed soil, and dissection of landscapes, causing irregular terrain, may well affect the results attained by automatic procedures. The ratio technique is implemented to suppress the influence of just such factors.

The approach taken in this research was to follow a strictly automatic procedure, basing as many of the decisions as possible on quantitative data. The six unique ERTS ratios were used simultaneously for automatic procedures involving ratio gating logic to recognize geologic targets. Information compiled from geologic and topographic maps, from geologic literature, and finally from a field trip were used for comparison with the resultant recognition. Detailed areal photointerpretation for structural detail was not attempted.

Prior to automatic recognition of the ERTS frame covering the entire Wind River Basin, a small subframe area near the Atlantic City Iron Mine was used for supervised training (see Figure 7). It was within this preliminary test site that each target class was defined.

Figure 10 is an analog ratio image (after dark object subtraction) of ERTS-MSS Channel 7/ Channel 4. The area is located on the southeastern extremity of the Wind River Mountains at the perimeter of the basin, as evidenced by the outcropping Paleozoic sediments dipping northeast in the image. Spotty, undrained lakes (in black) are characteristic of the rugged mountain country of Precambrian granite. Vigorous low vegetation delineating dendritic drainage which extends radially from the mountains comprises the brightest areas in the scene, having a high reflectivity in the infrared and relatively low reflectivity in the green. Two areas of specific geologic interest are the Triassic redbeds, the light-toned sediments cutting diagonally across the upper right corner, and the Atlantic City Iron Mine (in black in the lower right quadrant). In this ratio both of these targets were enhanced so that they could be easily distinguished from surrounding materials.

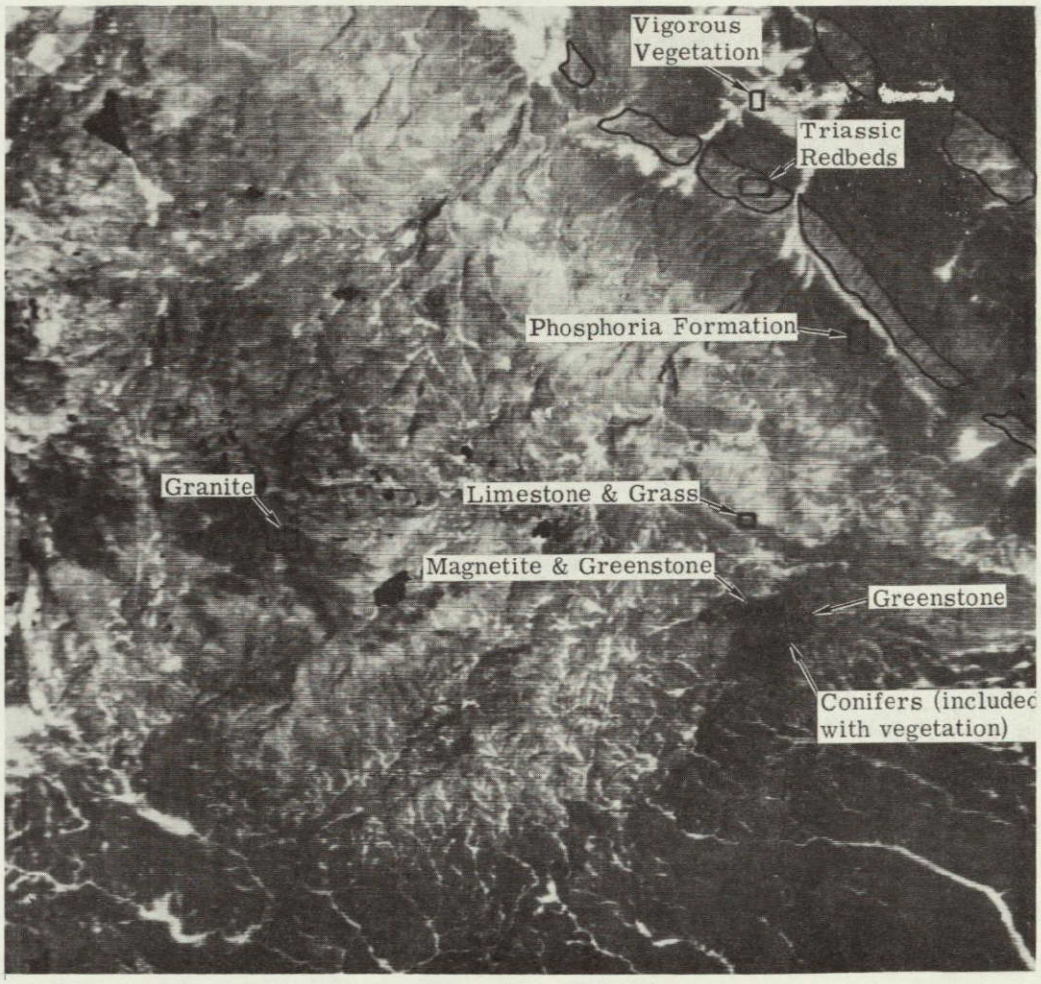

FIGURE 10. ERTS MSS CHAN 7/CHAN 4 OF SUB-FRAME TEST SITE NEAR ATLANTIC CITY, WYOMING WITH ANNOTATION OF TARGET REGIONS

Targets from the area shown in Figure 10 were selected on the basis of scanner imagery and geologic maps. The actual surface conditions of the target areas were not well-known at the time of processing, although it was assumed that vegetation influence over much of the area would be minimal for the August date chosen.

Extrapolation of these target selections to the entire Wind River Basin was inherently imperfect, in that many more possible materials were present than the six represented. The map produced, by necessity, group assemblages of surface compositions which are similar in spectral characteristics for ERTS-MSS bands. Each target class is represented by a separate color in the resultant recognition map in Figure 11.

Figure 12, showing recognition for the granite target alone, is a good example of the complexity of the resulting classification. Although some recognition of the target class is present where it was expected, in the Wind River Mountains, much of the recognition seems also to correlate with a major formation in the basin, the Tertiary Wind River Formation. Recognition within the boundaries of the Wind River Formation is shown in Figure 12 as orange. Other recognition is shown in white. The northern area of the Wind River Formation is well recognized; a major part of the southwestern exposure was not recognized. It is speculated that this lack of recognition is due to a facies change in this area and/or to overlying quaternary dune deposits. If so, the increased presence of the Puddle Springs arkose, a member of the Wind River Formulation, could be the cause of the differences in the southeastern part of the basin. Notably, the Puddle Springs arkose is the host rock of the roll-type uranium deposits of the Gas Hills District and its occurrences are important for uranium exploration.

Two targets were trained on areas of known dense vigorous vegetation. These are depicted in two shades of green on the color recognition composite (Figure 11), but were combined in Figure 13 to form one vegetation class. Recognition in orange (on Figure 13) corresponds to those areas also shaded as woods and brushland on the standard 1:250,000 U.S.G.S. topographic sheets. ERTS recognition appears to be more accurate at delineating areas of dense vegetation than the topographic sheets for most areas. This is not surprising, for the green overlay on such sheets is often old. (The overlay on the latest 1:250,000 sheets was prepared in 1961 and thus was not representative of present conditions.)

The recognition class containing magnetite and greenstone, shown in black on the color composite, was trained on the Atlantic City Iron Mine, owned by the United States Steel Corporation. The northeast-southwest trending ore body of Precambrian iron formation within Goldman-Meadows formation is exposed in the mine along with the Roundtop Mountain greenstone, also of Precambrian age. The iron formation is chiefly composed of quartz and magnetite, with a minor constituent of amphibole, and has an average thickness of 150 feet. Other exposed outcrops of iron formations known to be present in the area were not recognized due to their

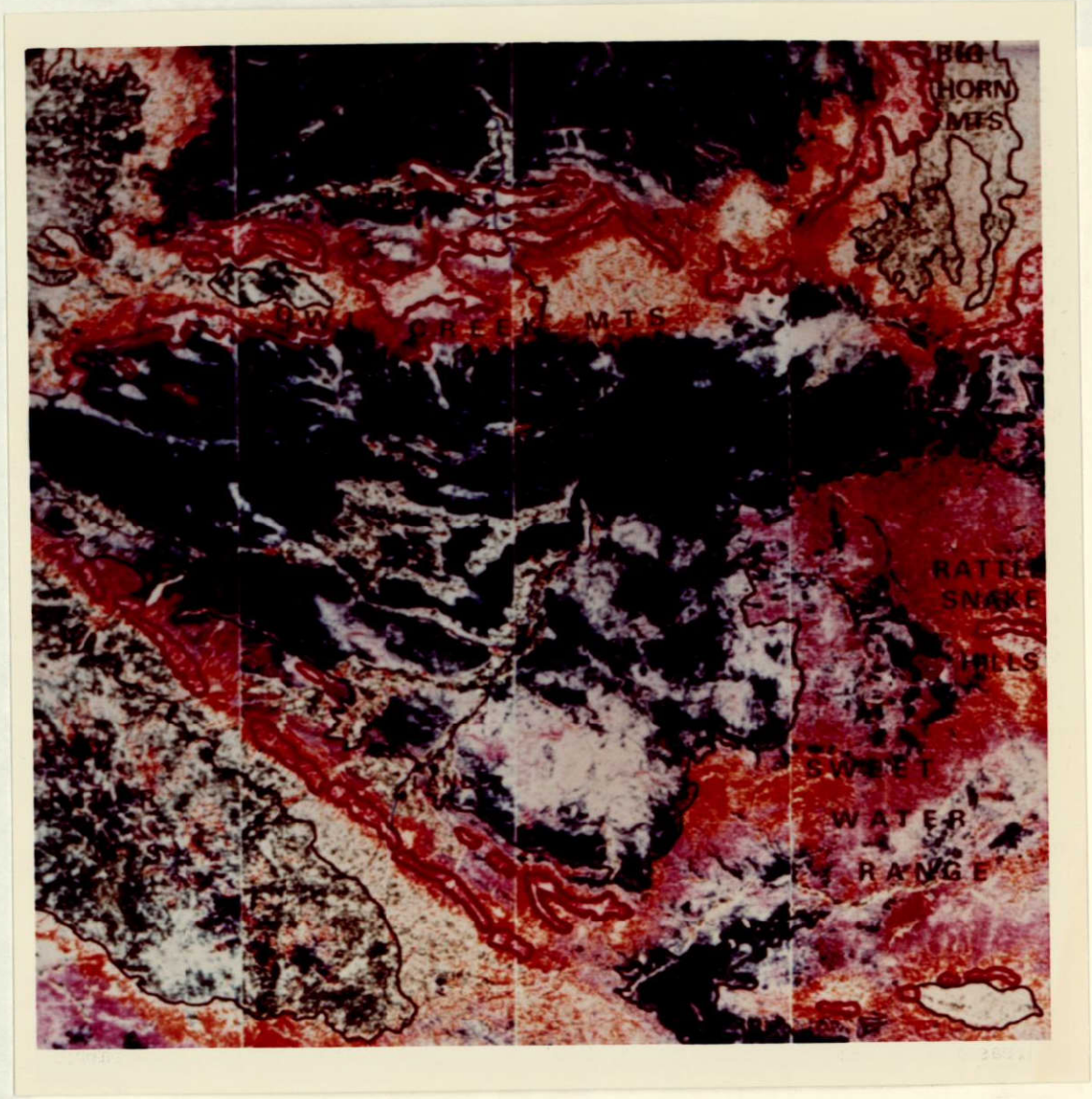

FIGURE 11. COLOR COMPOSITE OF CLASSIFICATION

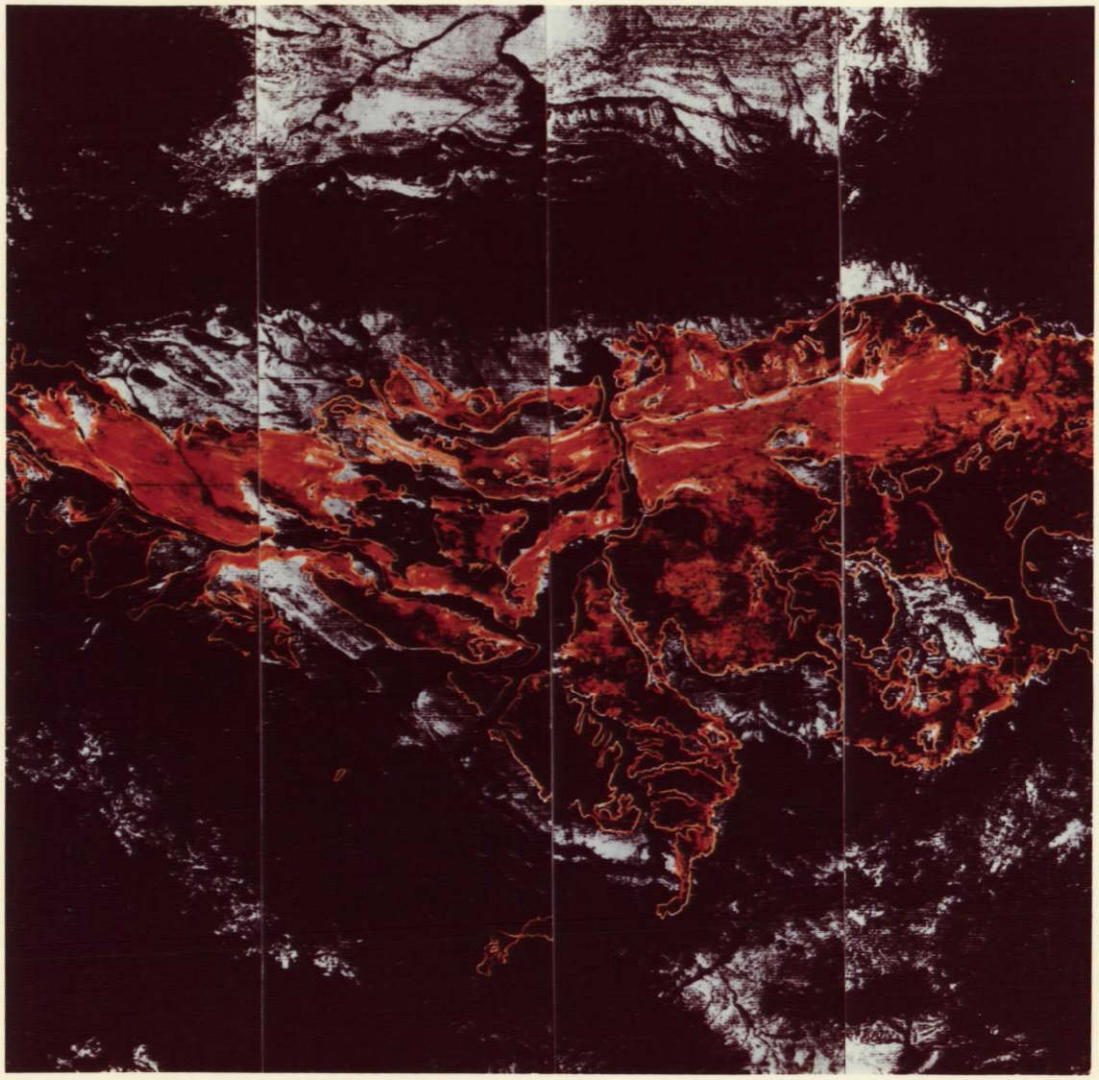

FIGURE 12. ERTS 6-RATIO INPUT AUTOMATIC RECOGNITION BY SUPERVISED TRAINING ON GRANITE. Orange-recognition within Tertiary Wind River Formation; White-other recognition, Wind River Basin, Wyoming.

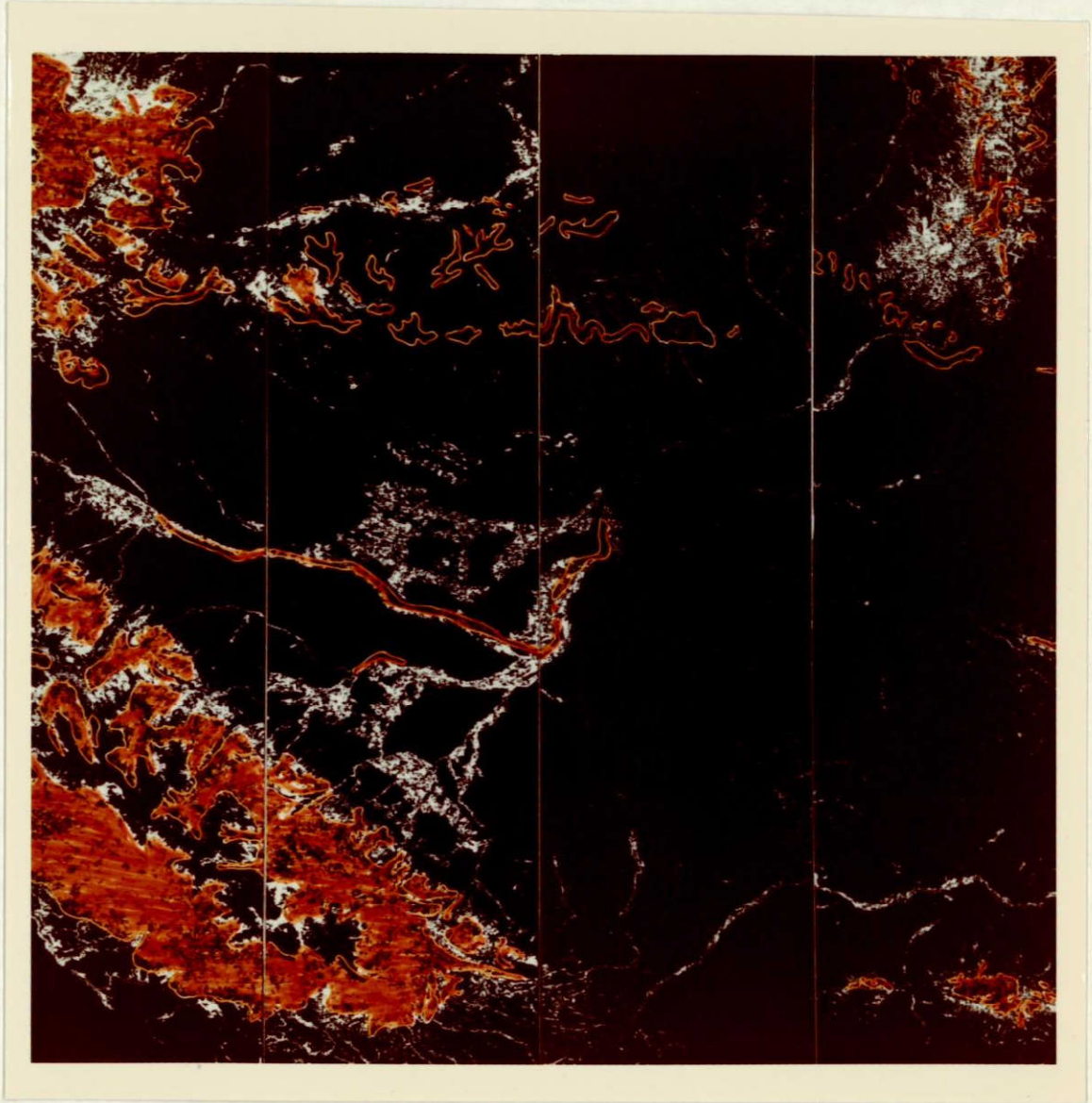

FIGURE 13. ERTS 6-RATIO INPUT AUTOMATIC RECOGNITION BY SUPERVISED TRAINING ON VEGETATION. Orange-recognition within area designated as woods and brushland on topographic map; White-other recognition, chiefly agriculture in river valleys, Wind River Basin, Wyoming.

limited size. However, the entire exposure of magnetite and greenstone in the mine was recognized. Incidental recognition was also found in areas of white snow, cloud and cloud shadow, and the dark gray pit bottoms of the uranium mines in the Gas Hills. It appears that this target class recognized those areas of slightly decreasing spectral reflectivity toward the infrared, generally causing ratio values of less than 1.

Other recognition targets resulted in varying degrees of success, although the controlling factors are not entirely understood. A good example of confused, yet not meaningless, recognition results can be seen in Figure 14. The target trained for this class was the normalization location on the Gallatin limestone (orange in Fig. 11). The two geologic units outlined and recognized in orange in Figure 14 are the Gallatin through Madison limestones, and the Tensleep formation, a calcareous sandstone. These were the areas which were expected to show the best recognition, but in the event recognition was localized and spotty. One obvious reason for this, which can be seen in a comparison of this recognition with that of dense vegetation (Fig. 13), was vegetative cover in some areas. Interestingly, the white recognition considered false-alarm recognition as presented here, does appear to be geologically controlled. At least part of the Phosphoria formation, made up of dolomites, limestones, and phosphatic shales and siltstones [21] seems to have been recognized. The Sundance formation which is known to undergo facies changes between its exposure along the Wind River range and that to the north of the basin, is also recognized in the south but not in the north.

The class actually trained on one area underlain by the Phosphoria formation is shown in Figure 15, and in purple in the color composite (see Fig. 11). Two formations other than the Phosphoria seem to have been recognized by this target, as well as the southeast region of the Wind River Formation. Both the Cloverly-Morrison formation and the Frontier formation are sandstones interbedded with finer sediments and are to be recognized in this class. The specific similarity among these geologic materials which has commanded their collective recognition has not been determined. More work in deciphering spectra of natural surface materials will lead to more definitive works in the future.

M. Dane Picard and others have studied the Triassic redbeds of the Wind River Basix extensively in order to determine their genetic significance for the Mesozoic paleogeography of the area. Most of the articles written are concerned with stratigraphic relationships and with lithologic terminology as it is significant for genetic theories on redbeds. Several articles, however, deal with the chemistry of certain members of the redbed units and report on relative concentrations of iron oxide, chiefly in the form of well-dispersed fine hematite coating sand grains and in matrix material. As reported by Picard [19]:

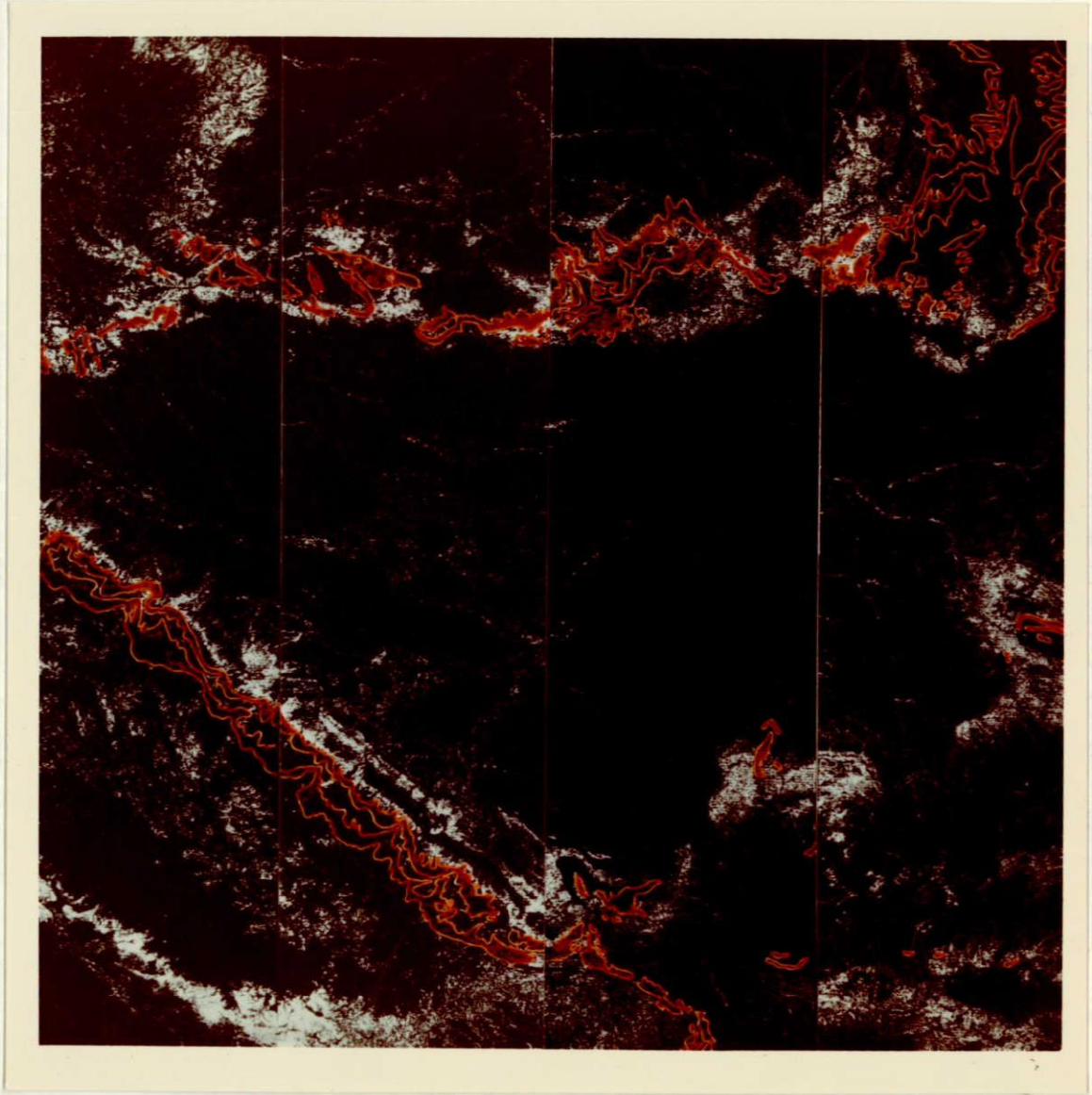

FIGURE 14. ERTS 6-RATIO INPUT AUTOMATIC RECOGNITION BY SUPERVISED TRAINING ON LIMESTONE. Orange-recognition with boundaries of Gallatin through Madison limestones and calcareous Tensleep Sandstone with geologic boundaries superimposed; White-other recognition, Wind River Basin, Wyoming.

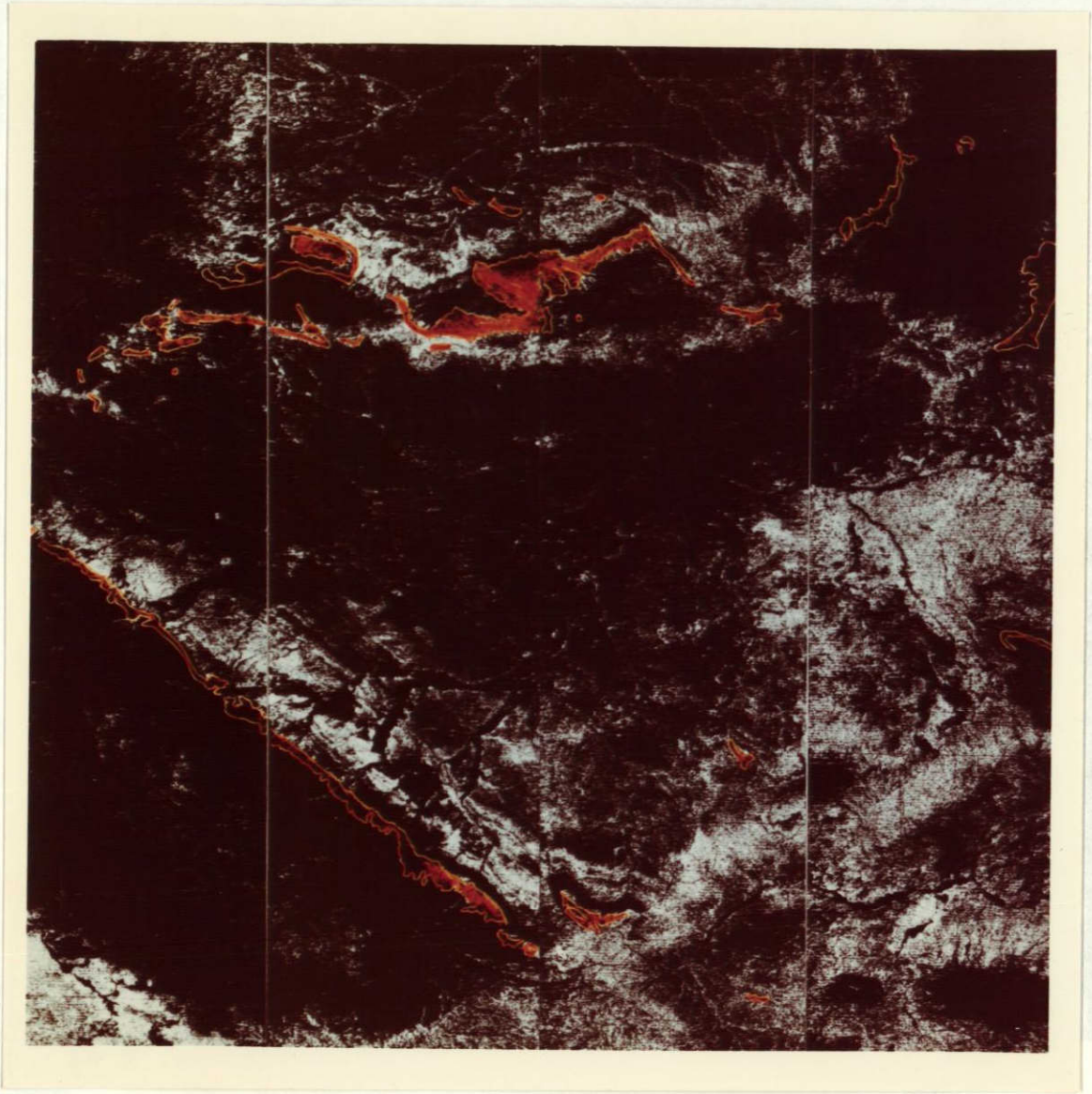

FIGURE 15. ERTS 6-RATIO INPUT AUTOMATIC RECOGNITION BY SUPERVISED TRAINING ON PHOSPHORIA FORMATION. Orange-recognition occurring within the Phosphoria Formation with geologic boundaries superimposed; White-other recognition, particularly good within the Cloverly-Morrison and Frontier formations, Wind River Basin, Wyoming.

"Hematite is the dominant opaque mineral [of the Red Peak and Crow Mountain Members of the Chugwater Formation of Triassic age], as noted by Van Houten (1961, p. 297), occurring in localized patches, in small veinlets and lenses, as pore space filler, as grain coatings, and as detrital grains. The detrital grains of hematite may be the products of alteration of detrital magnetite to hematite. Many of the detrital grains of hematite are rounded, and in some grains, red staining radiates a fraction of a millimeter outward from hematite grains. Hematite is greatly predominant over magnetite, and rounded hematite grains are more common than rounded magnetite grains."

It is the dispersed character of the red pigment materials of the Triassic redbeds and other oxide-stained formations that is important in mapping their occurrence from space imagery, or in recognizing their occurrence through automatic recognition. Although the relative percentage of iron is rather small (less than 5% for even the reddest rocks), its influence on the spectral response is disproportionately great. Also, since ERTS has a red channel (0.6-0.7 μm), chances for recognizing the influence of iron oxides on the basis of rock color are particularly good.

A sixth target covered the Triassic redbeds, and some of the pinkish Nugget formation as well. The spectral reflectance of this formation was unique in the scene and was seen to be so in the recognition. As the red color which was used for this target on the recognition composite in Figure 9 did not photograph well, it had to be manually enhanced. However, the accuracy of the target can be evaluated from its solitary display in Figure 16. For comparison, the outlines of mapped exposures of Triassic age redbeds have been superimposed, showing excellent correlation. Areas other than those mapped as Triassic redbeds which have been recognized throughout the scene are assumed to be other areas of predominantly red color.

In summary, this preliminary exercise is automatic recognition using multiple ratio inputs was successful for some specific targets, but not for all. Although recognition was not always predicted accurately, the results show that geologic features do control the spectra to the extent that, with more development, this approach may be a useful tool. The lack of information about surface conditions beyond the geologic mapping of exposed rocks was the limiting factor in our interpretation of the results. Selection of multispectral channels and the natural variety of surface materials being what they are, broad thematic mapping of geological materials will have to follow more reserved, concentrated studies on specific materials.

7
CONCLUSIONS

Examination of individual ratio images revealed that Triassic redbeds, siltstones and shales well exposed as red cuestas along the perimeter of the Wind River Basin, had uniquely bright

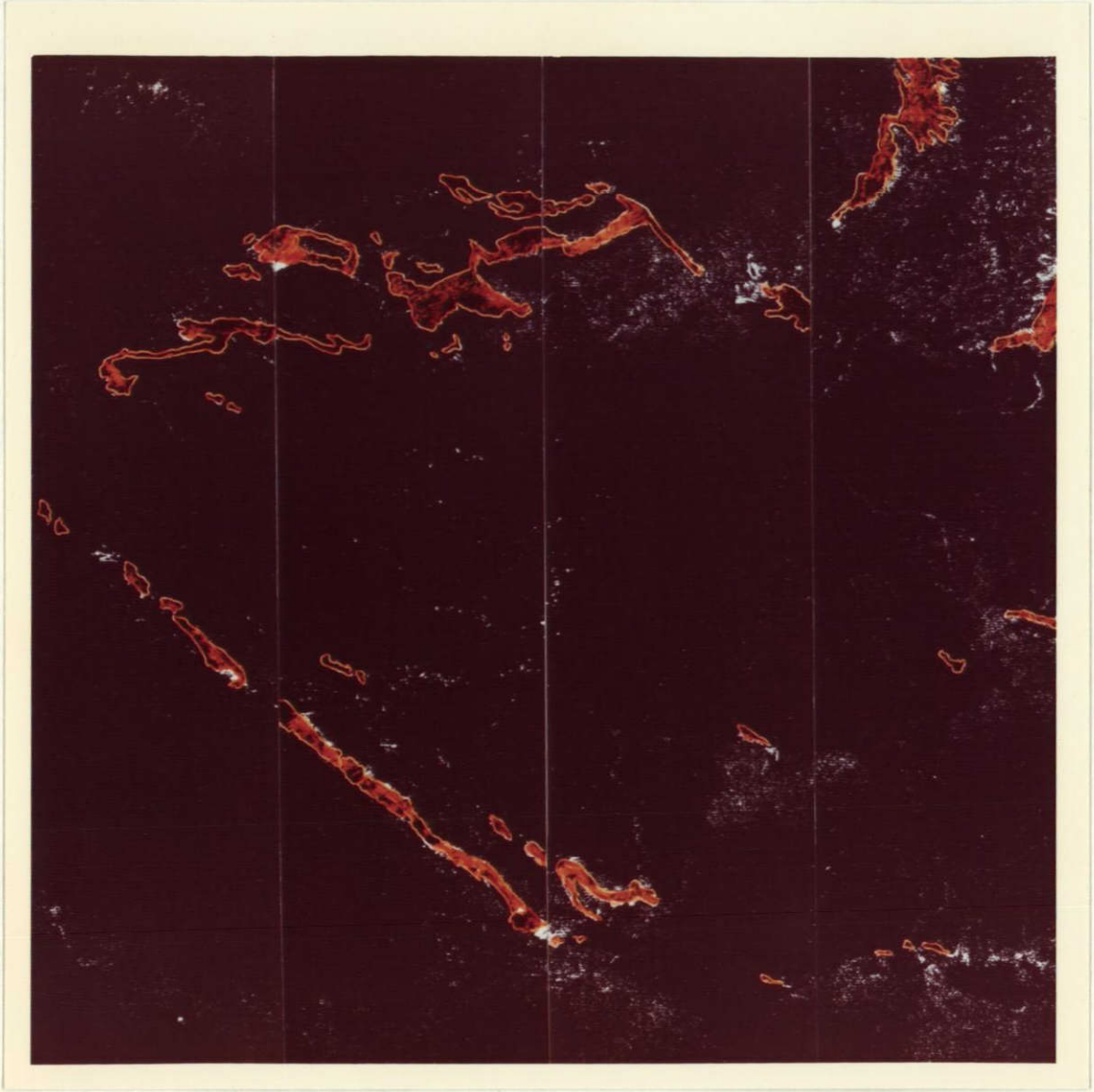

FIGURE 16. ERTS 6-RATIO INPUT AUTOMATIC RECOGNITION BY SUPERVISED TRAINING ON TRIASSIC REDBEDS. Orange-recognition within formation with geologic boundaries superimposed; White-other recognition, Wind River Basin, Wyoming.

tones in the red to green ratio image, $R_{5,4}$. Density slicing of this ratio showed that highest voltage levels produced brightest tones primarily at known exposures of the red Chugwater Formation. See Section 3.3 for further discussion.

Vigorous vegetation has the lowest dynamic voltage levels in the red/green ratios (except for water), because of its relatively high reflectance in the green and chlorophyll absorption in the red. Ratio values between the extremes of dense vegetation and exposed red Chugwater Formation are controlled by three factors: (a) relative reflectance in these two bands, which is assumed to correlate with some systematic color variation from green to red in the substrate; (b) the percentage of vegetation cover contributing increased reflectance in the green; and (c) the vigor of the vegetation, e.g., alive or dead. In the inner basin the amount of sage and bunch grass is assumed to be relatively uniform, except in those areas where recent drainage allows maximum vegetation cover. Variations in $R_{5,4}$ can then be attributed to differences in the substrate. This may be a valid assumption for the data presented, for there are evident variations correlating to known differences in geology.

Areas where the exposed rock or soil is red, orange or orange-yellow, indicating high reflectivities in the 0.6 to 0.7 μm region, should yield abnormally high values of $R_{5,4}$ ratio e.g., soils or rocks with well-disseminated colorful minerals such as hematite or limonite.

Reflectance data collected in the laboratory for various rocks and minerals were converted to single response-weighted reflectances for all four ERTS channels. The six non-reciprocal ratios possible from four channels of data were then calculated and grouped according to increasing ratio values. These data were used to establish signatures for in-scene training in supervised automatic pattern recognition. The procedure as it was attempted here was only partially successful. Incorrect estimates of vegetative cover in the normalization target were made due to limited groundtruth. Analysis of recognition maps was further impeded by lack of knowledge of terrain types discriminated in ratios of non-visible bands.

The $R_{5,4}$ ratio is fairly well understood because both channels are in the visible, and tones can be integrated by comparing them with colors. The interpretation of ratios formed from other ERTS channels is made more difficult because results cannot be compared with perceived color. Without this insight it is difficult to deduce the significance of recognition produced with six simultaneous ratios. A complicating factor is the use of a limited number of training sets. The full complexity of the scene may not be accounted for, and unrelated materials will thus be forced into the same recognition class. For these reasons, geologic targets other than redbeds were not easily separated into compositionally unique groups, although some were spectrally distinctive.

To evaluate the effectiveness of the ratio method for reducing atmospheric and solar illumination variations, spectral ratio maps of a subframe area were compared for two passes separated by 72 days. Two $R_{7,5}$ maps were merged and ratioed to form a temporal ratio map. Points that were expected not to vary between the two dates (those other than highly vegetated areas or cloud cover) were identified as ground invariant points. This $R_{7,5}$ temporal ratio with atmospheric corrections showed 37.30% of the ground invariant points changed less than ±5% and 96.83% changed less than ±15%. In comparison, 3.37% and 10.17% of ground invariant points in temporal ratios of MSS single channels 7 and 5 changed respectively less than ±5%. The temporal ratio of $R_{7,5}$ without atmospheric correction showed improvement over single channels to 21.02% of ground invariant points changing less than ±5%. The conclusion is that the ratio method produced a map which was less dependent on atmospheric and solar illumination than either the uncorrected ratio map or the maps of single channel radiances.

In summary, although the larger effort of this study was devoted to multi-ratio recognition, the most significant result for geologic investigations is the identification of the potential of red to green ratio. This success in detecting colorful iron compounds is dependent on strong absorption in the green by the presence of the Fe^{3+} ion with concomitant high reflectivity in the red. This spectral information is not necessarily adequately exploited by the wide bands of ERTS. Narrowing of those bands, with selective optimal placement for Fe^{3+} absorption features, should result in increased sensitivity and improve levels of detectability. Continued research investigating specific features of this and other ratios will result in the identification of more useful geologic applications as well as a refinement of requirements for future earth resource satellites.

REFERENCES

1. R. Turner, W. Malila and R.Nalepka, Importance of Atmospheric Scattering on Remote Sensing, or, Everything You've Always Wanted to Know About Remote Sensing but Were Afraid to Ask, Proceedings, Seventh International Symposium on Remote Sensing of Environment, Report No. 10259-1-X, Willow Run Laboratories of the Institute of Science and Technology, The University of Michigan, Ann Arbor, 1971.

2. R. K. Vincent, An ERTS Multispectral Scanner Experiment for Mapping Iron Compounds, Proceedings, Eighth International Symposium on Remote Sensing of Environment, Report No. 195600-1-X, Willow Run Laboratories of the Institute of Science and Technology, The University of Michigan, Ann Arbor, 1972.

3. F. J. Thomson, ERIM Progress Report on Use of ERTS-1 Data, Summary of Ten Tasks, Type II Progress Report, Report No. NASA-CR-133556, NTIS No. E73-10899/WR, Environmental Research Institute of Michigan, Ann Arbor, 1973.

4. K. R. Piech, and J. E. Walker, Interpretation of Soils, Photogram, Engin., Vol. XL, 1974, pp. 84-94.

5. V. Leeman, D. Earing, R. Vincent and S. Ladd, The NASA Earth Resources Spectral Information System: A Compilation, Report No. NASA-CR-31650-24-T, The University of Michigan, Ann Arbor, 1971.

6. V. Leeman, The NASA Earth Resources Spectral Information System: A Compilation, First Supplement, Report No. NASA CR-WRL-31650-69-T, Willow Run Laboratories of the Institute of Science and Technology, The University of Michigan, Ann Arbor, 1972.

7. R. K. Vincent, The NASA Earth Resources Spectral Information System: A Compilation, Second Supplement, Report No. NASA-CR-ERIM-31650-156-T, the Environmental Research Institute of Michigan, Ann Arbor, 1973.

8. A. Locke, Leached Outcrops as Guides to Copper Ore, Williams and Wilkins, Baltimore, 1926.

9. H. B. Weiser, The Hydrous Oxides, McGraw-Hill Book Co., Inc., New York, 1926, pp. 70-74.

10. R. Blanchard, Interpretation of Leached Outcrops, Nevada Bureau of Mines Bulletin 66, University of Nevada, 1968.

11. W. C. Kelly, Topical Study of Lead-Zinc Gansans, Bulletin 46, State Bureau of Mines and Mineral Resources, New Mexico Institute of Mining and Technology, Socrro, New Mexico, 1958, pp. 42-47.

12. L. C. Rowan, P. H. Wetlaufer, A. F. H. Goetz Jr., F. C. Billingsly and J. H. Stewart, Discrimination of Rock Types and Detection of Hydrothermally Altered Areas in South-Central Nevada by the Use of Computer-Enhanced ERTS Images, U.S. Geological Survey Professional Paper 883, 1974, in press.

13. P. N. Shockey, R. I. Rackley and M. P. Dahill, Source Beds and Solution Fronts: Remarks to Wyoming Metals Section, AIME, 27 February 1958, 8 pages.

14. R. I. Rackley, "Environment of Wyoming Tertiary Uranium Deposits," Amer. Assoc. of Pet. Geolo. Bul., Vol. 56, 1973, pp. 755-77.

15. R. B. Krauskopf, Introduction to Geochemistry, New York, McGraw-Hill Book Company, New York, 1967. (International Series, Earth and Planetary Science) 721 p.

16. T. J. Donovan, "Petroleum Microseepage at Cement Oklahoma: Evidence and Mechanism, "Amer. Assoc. of Pet. Geolo. Bul., Vol. 58, pp. 429-446, 1974.

17. J. D. Love, "Stratigraphy and Correlation of Triassic in Central Wyoming," Twelfth Annual Field Conference, Wyoming Geological Association Guidebook, 1957, pp. 39-45.

18. M. D. Picard, "Stratigraphy and Depositional Environments of the Red Peak Member of the Chugwater Formation (Triassic), West-Central Wyoming," Wyoming University Contributions to Geology, Vol. 6, No. 1, Winter, 1967, pp. 39-67.

19. M. D. Picard, "Iron Oxides and Fine-Grained Rocks of Red Peak and Crow Mountain Sandstone Members, Chugwater (Triassic) Formation, Wyoming," Journal of Sedimentary Petrology, Vol. 35, No. 2, June 1965, pp. 464-479.

20. W. R. Keefer, "Geology of Petroleum in Wind River Basin, Central Wyoming," Amer. Assoc. of Pet. Geolo. Bull., Vol. 53, No. 9, September 1969, pp. 1839-1865.

21. R. E. Roadifer, Catalog of Formation Names for Southwestern Wind River Basin, in Wyoming Geological Association Guidebook: Southwest Wind River Basin, 1957.

22. W. R. Keefer, and E. I. Rich, "Stratigraphy of the Cody Shale and Younger Cretaceous and Paleocene Rocks in the Western and Southern Parts of the Wind River Basin, Wyoming," Wyoming Geological Association Guidebook: Southwest Wind River Basin, 1957.

23. N. M. Denson, and G. N. Pipiringos, "Stratigraphic Implications of Heavy Mineral Studies of Paleocene and Eocene Rocks of Wyoming," Twenty-First Annual Field Conference, Wyoming Geological Association Guidebook, 1969, pp. 9-18.

24. F. B. Van Houten, "Tertiary Rocks of Southern Wind River Basin Area, Central Wyoming," Wyoming Geological Association Guidebook: Southwest Wind River Basin, 1957.

25. G. Bressanian, et al., Data Preprocessing Systems for Earth Resources Surveys: Vol. II, Methods of Implementation, ESRO Report No. CR-296, Telespazio, Rome, Italy, September 1973, pp. 15-3 - 15-12.

BIBLIOGRAPHY

Anderson, D. C., "Uranium Deposits of the Gas Hills," Contributions to Geology (Wyoming Uranium Issue), Vol. 8, No. 2, Pt. 1, 1969, pp. 93-103.

Armstrong, F. C., "Geologic Factors Controlling Uranium Resources in the Gas Hills District, Wyoming," Wyoming Geological Association Guidebook, 1970: Wyoming Sandstone Symposium, pp. 31-44.

Blanchard, R. Interpretation of Leached Outcrops, Nevada Bureau of Mines Bulletin 66, University of Nevada, 1968.

Denson, N. M. and G. N. Pipiringos, "Stratigraphic Implications of Heavy Mineral Studies of Paleocene and Eocene Rocks of Wyoming," Twenty-First Annual Field Conference, Wyoming Geological Association Guidebook, 1969, pp. 9-18.

Dillman, R. and R. K. Vincent, Unsupervised Mapping of Geologic Features and Soils in California. Proceedings of the Ninth Symposium for Remote Sensing of Environmental, the Environmental Research Institite of Michigan, Ann Arbor, 1974, pp. 2013-2025.

Donovan, T. J., "Petroleum Microseepage at Cement Oklahoma: Evidence and Mechanism," Amer. Assoc. Pet. Geolo. Bul., Vol. 58, 1974, pp. 429-446.

Groth, F. A., "New Sandstone Uranium Deposit in the Battle Spring Formation, Lost Soldier - Green Mountain Area, Sweetwater County, Wyoming," Twenty-Second Annual Field Conference, Wyoming Geological Association Guidebook, 1970, pp. 9-12.

Houston, R. S., "Aspects of the Geologic History of Wyoming Related to the Formation of Uranium Deposits," Contributions to Geology (Wyoming Uranium Issue), Vol. 8, No. 2, Pt. 1, 1969, pp. 67-79.

Hovis, W. A., Jr. and W. R. Callahan, "Infrared Reflectance Spectra of Igneous Rocks, Tuffs, and Red Sandstone from 0.5 to 22 Microns," Applied Optics, Vol. 5, No. 2, 1966, pp. 245-248.

Hunt, G. R., J. W. Salisbury and C. J. Lenhoff, "Visible and Near-Infrared Spectra of Minerals and Rocks, No. V: Halides, Phosphates, Arsenates, Vanadates, and Borates," Modern Geology, Vol. 3, 1972, pp. 121-132.

Keefer, W. R. and E. I. Rich, Stratigraphy of the Codey Shale and Younger Cretaceous and Paleocene Rocks in the Western and Southern Parts of the Wind River Basin, Wyoming," Wyoming Geological Association Guidebook: Southwest Wind River Basin, 1957.

Keefer, W. R., "Geology of Petroleum in Wind River Basin, Central Wyoming," Amer. Assoc. of Pet. Geol. Bul., Vol. 53, No. 9, September 1969, pp. 1839-1865.

Kelley, W. C., Topical Study of Lead-Zinc Gansans, Bulletin 46, State Bureau of Mines and Mineral Resources, New Mexico Institute of Mining and Technology, Socrro, New Mexico, 1958, pp. 42-47.

Krauskoph, R. B., Introduction to Geochemistry, New York, McGraw-Hill Book Company, New York, 1967 (International Series, Earth and Planetary Science) 721 p.

Leeman, V., D. Earing, R. Vincent and S. Ladd, The NASA Earth Resources Spectral Information System: A Compilation, Report No. NASA CR-31650-24-T, Willow Run Laboratories of the Institute of Science and Technology, The University of Michigan, Ann Arbor, 1971.

Leeman, V., The NASA Earth Resources Spectral Information System: A Compilation, First Supplement, Report No. NASA CR-WRL-31650-69-T, Willow Run Laboratories of the Institute of Science and Technology, The University of Michigan, Ann Arbor, 1972.

Locke, A., Leached Outcrops as Guides to Copper Ore, Williams and Wilkins, Baltimore. 1926.

Love, J. D., Preliminary Report on Uranium in the Gas Hills Area, Fremont and Natrona Counties, Wyoming, U.S. Geological Survey Circular 352, 1954.

Love, J. D., "Stratigraphy and Correlation of Triassic in Central Wyoming," Twelfth Annual Field Conference, Wyoming Geological Association Guidebook, 1957, pp. 39-45.

Lyon, R. J. P., Evaluation of IR Spectrophotometry for Compositional Analysis of Lunar and Planetary Soils: Rough and Powdered Surfaces, Final Report, Part II, NASA Contract NASr-49(04), Stanford Research Institute, Menlo Park, 1964.

Picard, M. D., "Iron Oxides and Fine-Grained Rocks of Red Peak and Crow Mountain Sandstone Members, Chugwater (Triassic) Formation, Wyoming," Journal of Sedimentary Petrology, Vol. 35, No. 2, June 1965, pp. 464-479.

Picard, M. D., "Stratigraphy and Depositional Environments of the Red Peak Member of the Chugwater Formation (Triassic), West-Central Wyoming," Wyoming University Contributions to Geology, Vol. 6, No. 1, Winter 1967, pp. 39-67.

Piech, K. R. and J. E. Walker, "Interpretation of Soils," Photogram, Engin., Vol. XL, 1974, pp. 84-94.

Rackley, R. I., "Environment of Wyoming Tertiary Uranium Deposits," Amer. Assoc. Pet. Geolo. Bul., Vol. 56, 1973, pp. 755-77.

Reinhardt, E. V., "Practical Guides to Uranium Ores on the Colorado Plateau," RMO-1027, U.S. Atomic Energy Commission Technical Information Service, Oak Ridge, Tennessee, 1952.

Roadifer, R. E., Catalog of Formation Names for Southwestern Wind River Basin in Wyoming Geological Association Guidebook: Southwest Wind River Basin, 1957.

Rowan, L. C., "Near Infrared Iron Absorption Bands: Applications to Geologic Mapping and Mineral Exploration, Fourth Annual Earth Resources Program Review," Vol. III, Sec. 60, Johnson Space Center, National Aeronautics and Space Administration, 1972.

Rowan, L. C., P. H. Wetlaufer, A. F. H. Goetz, F. C. Billingsly and J. H. Stewart, Discrimination of Rock Types and Detection of Hydrothermally Altered Areas in South-Central Nevada by the Use of Computer-Enhanced ERTS Images, U.S. Geological Survey Professional Paper 883, 1974, in press.

Salmon, B. C. and R. K. Vincent, Surface Compositional Mapping in the Wind River Range and Basin, Wyoming, by Multispectral Techniques Applied to ERTS-1 Data, Proceedings of the Ninth International Symposium on Remote Sensing of Environment, the Environmental Research Institute of Michigan, Ann Arbor, 1974, pp. 2005-2012.

Salisbury, J. W. and G. R. Hunt, Remote Sensing of Rock Type in the Visible and Near Infrared, Proceedings of the Ninth International Symposium on Remote Sensing of Environment, the Environmental Research Institute of Michigan, Ann Arbor, 1974, pp. 1953-1958.

Shockey, P. N., R. I. Rackley and M. P. Dahill, Source Beds and Solution Fronts: Remarks to Wyoming Metals Section, AIME, 27 February 1958, 8 p.

Thomson, F. J., ERIM Progress Report on Use of ERTS-1 Data, Summary of Ten Tasks, Type I, Report No. NASA-CR-ERIM 193300-24-L, Environmental Research Institute of Michigan, Ann Arbor, 1973.

Thomson, F. J., ERIM Progress Report on Use of ERTS-1 Data, Summary of Ten Tasks, Type II Progress Report, Report No. NASA-CR-133556, NTIS No. E73-10899/WR, Environmental Research Institute of Michigan, Ann Arbor, 1973.

Travis, R. B., "Classification of Rocks," Quarterly of the Colorado School of Mines, Vol. 50, No. 1, 1955, p. 12.

Turner, R., W. Malila and R. Nalepka, Importance of Atmospheric Scattering on Remote Sensing, or, Everything You've Always Wanted to Know About Remote Sensing but Were Afraid to Ask, Proceedings, Seventh International Symposium on Remote Sensing of Environment, Report No. 10259-1-X, Willow Run Laboratories of the Institute of Science and Technology, The University of Michigan, Ann Arbor, 1971.

Van Houten, F. B., "Tertiary Rocks of Southern Wind River Basin Area, Central Wyoming," Wyoming Geological Association Guidebook: Southwest Wind River Basin, 1957, pp. 79-88.

Vickers, R. C., "Alteration of Sandstone as a Guide to Uranium Deposits and Their Origin, Northern Black Hills, S. Dakota," Economic Geology, Vol. 52, No. 6, 1957, pp. 599-611.

Vincent, R. K., An ERTS Multispectral Scanner Experiment for Mapping Iron Compounds, Proceedings, Eighth International Symposium on Remote Sensing of Environment, Report No. 195600-1-X, Willow Run Laboratories of the Institute of Science and Technology, The University of Michigan, Ann Arbor, 1972, pp. 1239-1247.

Vincent, R. K., F. Thomson and K. Watson, "Recognition of Exposed Quartz Sand and Sandstone by Two-Channel Infrared Imagery," J. of Geophys. Res., Vol. 77, 1972, pp. 2473-77.

Vincent, R. K. and F. Thomson, "Rock Type Discrimination from Ratioed Infrared Scanner Images of Pisgah Crater, California," Science, Vol. 175, 1972, pp. 986-88.

Vincent, R. K., Rock-Type Discrimination from Ratio Images of Pisgah Crater, California, Report No. NASA-CR-ERIM 31650-77-T, Willow Run Laboratories of the Institute of Science and Technology, The University of Michigan, Ann Arbor, 1972.

Vincent, R. K., The NASA Earth Resources Spectral Information System: A Compilation, Second Supplement, Report No. NASA-CR-ERIM-31650-156-T, Environmental Research Institute of Michigan, Ann Arbor, 1973.

Vincent, R. K., Mapping Exposed Silicate Rock Types and Exposed Ferric and Ferrous Compounds from a Space Platform, EREP Investigation 444M, NASA, Houston, Texas, 1973.

Vincent, R. K., T. Wagner, B. Drake and P. Jackson, Geologic Reconnaissance and Lithologic Identification by Remote Sensing, Report No. 191700-8-F, Environmental Research Institute of Michigan, Ann Arbor, 1973.

Vincent, R. K., A Thermal Infrared Ratio Imaging Method for Mapping Compositional Variations Among Silicate Rock Types, Ph.D. Dissertation, Department of Geology and Mineralogy, The University of Michigan, Ann Arbor, 1973.

Vincent, R. K , G. Thomas and R. Nalepka, Signature Extension Studies, Report No. NASA-CR-ERIM 190100-26-T, Environmental Research Institute of Michigan, Ann Arbor, (in press).

Vine, J. D. and E. B. Tourtelot, "Preliminary Geochemical and Pertrographic Analysis of Lower Eocene Fluvial Sandstones in the Rocky Mountain Region," Wyoming Geological Association Guidebook: Wyoming Sandstones Symposium, 1970, pp. 251-263.

Wagner, T., R. K. Vincent, B. Drake, R. Mitchell and P. Jackson, Tunnel-Site Selection by Remote Sensing Techniques, Report No. 10018-13-F, Willow Run Laboratories of the Institute of Science and Technology, The University of Michigan, Ann Arbor, 1972.

Weiser, H. B., The Hydrous Oxides, McGraw-Hill Book Co., Inc., New York, 1926.